Innovations in Rotary Drill Bit Design to Reduce Vibration and Improve Durability

by

Omid Aminfar

A thesis
presented to the University of Waterloo
in fulfillment of the
thesis requirement for the degree of
Master of Applied Science
in
Mechanical Engineering

Waterloo, Ontario, Canada, 2008

AUTHOR'S DECLARATION

I hereby declare that I am the sole author of this thesis. This is a true copy of the thesis, including any required final revisions, as accepted by my examiners.

I understand that my thesis may be made electronically available to the public.

Abstract

Well drilling is an important process for extracting oil, natural gas, water, and mineral materials. Opening wells requires boring through earth formations, which can range from very soft to very hard. Penetrating into such formations requires specialized tools and operation procedures which should be employed based on the environment and application. Rotary drilling, in which a drill bit is used to crush the rock and penetrate into the formation, is one of the main methods of well drilling. Rotary cone bits are one of the main types of drill bits used for rotary drilling.

There are two main problems encountered when drilling with rotary cone bits. Excessive vibration can cause damage to the entire system and can decrease efficiency of the drilling process. Failure of the bit's bearings and seals can also result in damage to the bit and cessation of the drilling process. In recent years, a great deal of research has been undertaken to address these problems and find appropriate solutions to improve drilling efficiency and production rate while reducing the overall cost of drilling.

In this thesis, a new design for rotary cone bits, with the objective of improving overall drilling performance, is presented. First, a new pattern for distribution of inserts over the cone is presented, which results in reduced vibration of the drillstring. Second a new design for the bit's bearings is introduced that is capable of operating in harsh environments. Finally, an experimental set-up is introduced to evaluate the performance of the proposed designs.

Acknowledgements

I would like to express my genuine appreciations to my supervisor, Professor Amir Khajepour for his guidance, understanding, patience, and kindness throughout my research. I learned a great deal from his knowledge, character, and behaviour.

I warmly thank my former colleagues, Mrs. Shahrzad Towfighian and Mr. Jason Sears, whose assistance helped me to pursue my research.

I sincerely thank my former and current roommates, Ehsan Fathi, Edouard Tissier, Amod Gupta, Saman Mohammdi, and Soroosh Hassanpoor. Those times I lived with them have been wonderful moments in which I learned a lot about life.

My special thanks to all my friends who helped me during this important step of my life and with whom I spent joyful times: Hamidreza Alemohammad, Arash Tajik, Pedram Hassanzadeh, Nasser Lashgarian, Jaho Seo, Mehrdad Iravani, Hossein Bagheri, Amir Fazeli, Mahsa Moshrefi, Luke Ng, Harry Ng, Michele Heng and other kind friends of mine. I am also grateful to my friends in Iran and elsewhere who continued their friendships with me honestly.

I am especially thankful to Mrs. Sarah Mask who kindly proofread my thesis.

I would like to thank all the staff at the University of Waterloo who gave me this opportunity to learn, grow, and look at the world in a kinder and wiser way.

The financial support from Ontario Centers of Excellence (OCE) and ROTACAN is also appreciated.

Above all, I am deeply grateful to my loving family, my parents Mrs. Akram Soghandi and Mr. Mohammad Javad Aminfar, my brothers Hadi and Mehdi, and my sister Mojgan for their immortal love and support, which always shined on me far from home.

Dedication

This work is dedicated to my dearest people in the world:

my parents, Mrs. Akram Soghandi and Mr. Mohammad Javad Aminfar, my brothers Hadi and Mehdi, and my sister Mojgan: Love you all forever.

Table of Contents

List of Figures

List of Tables

Chapter 1
Introduction

1.1 Outline

In this chapter, the drilling process and its required tools are briefly reviewed. The concept of rotary drilling, the drilling assembly and its main parts are explained. Two major challenges encountered in well drilling are described; the objective of the research described in this thesis is to address these challenges to improve the overall drilling process performance.

1.2 Drilling Assembly

Well drilling is an important process for extracting oil, natural gas, water, and mineral materials. Opening wells requires boring through earth formations, which can range from very soft to very hard. Penetrating into such formations requires specialized tools and operation procedures which should be employed based on the environment and application. Rotary drilling, in which a drill bit is used to crush the rock and penetrate into the formation, is one of main methods of well drilling. Rotary cone bits are one of the main types of drill bits used for rotary drilling.

The rotary drilling process consists of two major steps: “penetrating into the rocks” and “removing the rock chips”. The first step generally involves crushing or shearing actions, which produce rock chips. The crushing or shearing is performed by means of special cutters installed on the drill bit which are pushed downward while drilling. To proceed in the drilling process, the generated rock chips must be extracted to the surface. The extraction of the rock chips is accomplished by using a special fluid that flushes out of the drill bit and travels up through the annulus of the borehole and the drillstring, bringing the waste rock to the surface.

The drill rig is a machine used to drill boreholes in the ground. This machine accommodates the vertical and rotational motion of the drillstring and circulates the drilling fluid. The main parts of a drill rig are the derrick, rotary table, drillstring, and drill bit. The derrick is a structure which is used to support the drillstring. The rotary table provides the required torque to turn the drillstring. The drill bit and the drillstring are the main tools which perform the drilling and penetrating steps. Figure 1-1 shows a sample oil drill rig with its main components and Figure 1-2 shows the drilling fluid circulation process:

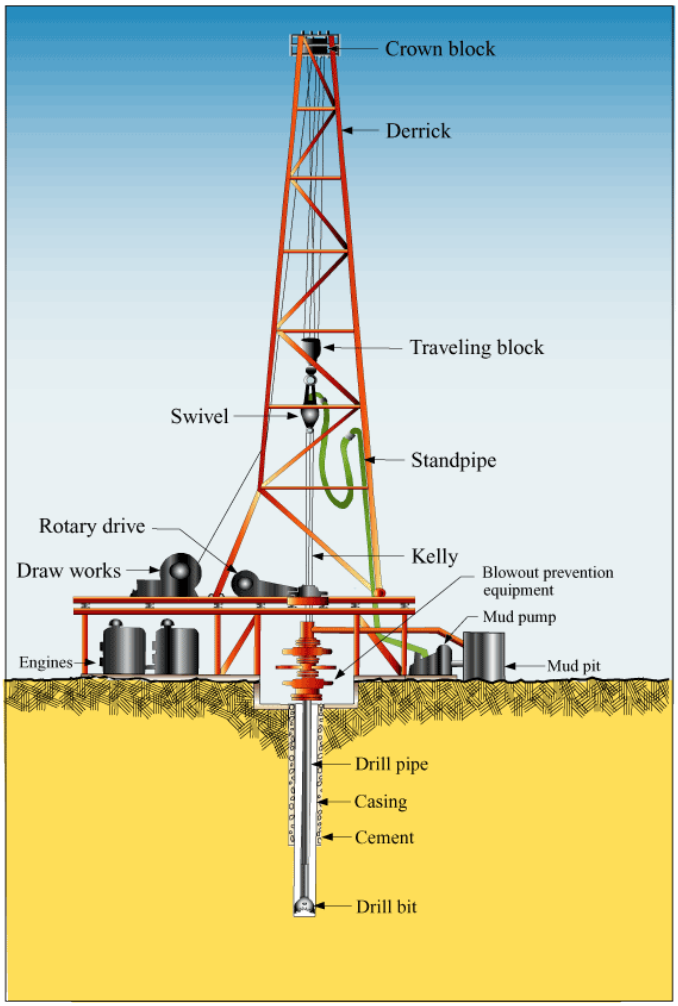

Figure 1-1: A sample oil drill rig (California Department of Conservation)

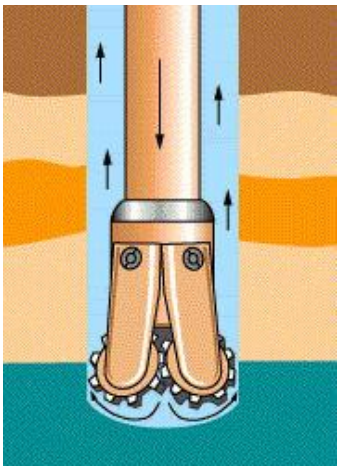

Figure 1-2: Drilling fluid circulation (Production Enhancement Systems)

The drillstring is a long tube consisting of drill pipes, drill collars, stabilizers, and other downhole equipment. The main function of this system is to transmit the rotary motion generated by the rotary table to the drill bit downhole. It also provides the axial force required for crushing rock and penetrating into the formation; this force is known as weight-on-bit (WOB) and can be induced by either the weight of the drillstring or by the hydraulic cylinders uphole. The length of drillstrings differs due to their various applications; for blasthole drilling, it possesses a short length and is comprised of a number of drill pipes connected to the drill bit at their end bottom, as shown in Figure 1-3, while for oil well drilling the entire length can exceed thousands of meters and it consists of drill pipes, drill collars, and stabilizers. In both cases, the drill pipes or drill collars are fed to the drillstring while boring into the ground.

Figure 1-3: A blasthole drill rig (Sandvik)

Drill pipes and drill collars are the main components of a drillstring. Although both of these are steel tubular components, the drill collars have a thicker wall. In blasthole drilling, drill pipes constitute the whole length of the drillstring; whereas for oil well drillstrings, they form the majority of the length of the drillstring from the surface to a distance close to the drill bit. In the latter case, the remainder of the drillstring is called the bottomhole assembly (BHA), which has a dominant influence on the drillstring's performance. Drill collars are the main elements of the BHA and can provide the required weight on the bit for drilling. Some other downhole equipment, such as measurement tools and shock absorbers, are also connected to the BHA.

The drill bit, which crushes the rock and penetrates into the formation, is mostly comprised of drilling cutters installed on a rotating element that are capable of crushing or shearing rock. The drill bit is attached to the bottom end of the drillstring and receives the rotary motion and downward force transmitted by the drillstring. A fluid consisting of mostly air or special liquids is ejected from the bit's nozzles to the borehole to extract the cutting chips to the surface through the annulus between the borehole wall and the drillstring.

The two main types of drill bits used are the rotary cone (RC) bits and the polycrystalline diamond compact (PDC) bits. A rotary cone bit, as shown in Figure 1-4, consists of three cones which are mounted on their assigned arms. The arms are welded together forming the body of the bit. The outside area of the cones is covered by different rows of hard-material inserts, which are used for crushing the rocks. Figure 1-5 illustrates the components of a rotary cone bit. Bearings located between the inside cavity of the cone and the arm's journal shaft allowing the cones to rotate freely. While operating, the cutters crush the rock due the elevated force applied downwardly; this action is repeated all over the formation when the bit turns.

Figure 1-4: Rotary cone bit (ROTACAN)

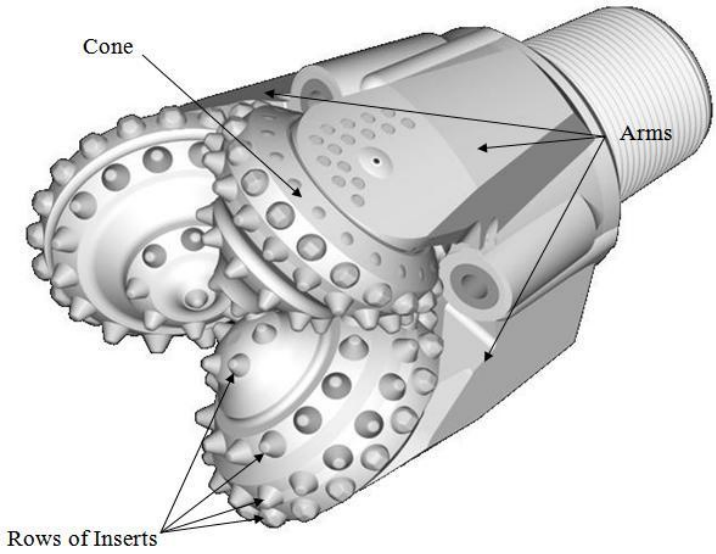

Figure 1-5: Components of a rotary cone bit (ROTACAN)

PDC bits use a dragging or shearing action and do not have any rotating elements. The cutters are installed on the body of the bit and shear the rock and generate rock chips. This type of bit is generally used in soft and medium-hard formations; however, the rotary cone bits are more desirable for hard formations. Figure 1-6 shows a typical PDC bit.

Figure 1-6: PDC bit (Baker Hughes)

1.3 Rotary Drilling Challenges

There are two main problems encountered when drilling with rotary cone bits. Excessive vibration of different parts of the drilling assembly can cause damage to the entire system and decrease the efficiency

of the drilling process. Failure of the bit's bearings and seals can result in damage to the bit and cessation of the drilling process. In recent years, a great deal of research has been undertaken to address these problems and find appropriate solutions to improve drilling efficiency and production rate while reducing the overall cost of drilling.

Vibrations have been reported to have a significant detrimental effect on drilling performance. They affect weight on bit (WOB), rate of penetration (ROP), and drilling direction and can also cause severe damage to drilling tools, such as bottomhole assemblies (BHA), measurement while drilling (MWD) tools, cutters, and bearings. They can also reduce efficiency of drilling by absorbing some of the total energy transmitted downhole.

Failure of the bearings is one of the main causes of damage to the drill bits. Hard formations and system vibrations may generate elevated forces and shocks resulting in damage to the bearings. Due to the presence of drilling mud and the rock chips produced while drilling, the bearings must be sealed off from the external environment. These seals are also facing some challenges which make it difficult to maintain the efficiency of the seals. The high temperature generated by the friction of the bearing surfaces, as well as the high temperature of the earth in deep wells, add to the overall bit's temperature and can affect seal's performance. Elevated pressure may also result in premature damage to the seal, while can result in debris and the drilling liquid seeping into the bearing's cavity, which prevents the bearings from functioning properly. This situation commonly occurs in very deep wells, where the heavy drilling mud circulating through the drillstring can generate a considerable pressure on the seal's face.

In this thesis, we present new designs to overcome the aforementioned problems with the objective of improving overall drilling performance. First, a new pattern for distribution of inserts over the cone is presented which results in reduced vibrations of the drillstring. Second, a new design for the bit's bearings is introduced, which is capable of operating in harsh environments. Finally, an experimental set-up has been designed which can be used to evaluate the performance of the proposed designs.

First, a literature review on drillstring vibrations and rotary drill bit's bearing and seal designs is presented in Chapter 2. The first part of the thesis, which deals with the insert pattern optimization, is described in Chapters 3 to 6. Chapter 3 describes the mathematical basics required to determine the overall system's response. The proposed drillstring and excitation models are introduced in Chapter 4. The optimization procedure is described in 0Chapter 5 . Final results are presented in Chapter 6.

The second part of the thesis, which deals with the bearing and seal design, is presented in Chapters 7 to 9. The required definitions and formulas for designing tapered roller bearings are described in Chapter 7. Chapter 8 includes the analysis and design of new tapered bearings. The integrated design for the new

sealed tapered roller bearings is presented in Chapter 9. As the last part of this thesis, the experimental set-up used to evaluate the performance of the proposed designs is described in Chapter 10. Final discussions and recommendations are presented in Chapter 11.

Chapter 2
Literature Review

2.1 Outline

In this chapter, a literature review on drillstring vibrations and rotary drill bit's bearing and seal designs is presented. In the first section, three modes of vibrations of drillstrings are reviewed. Mathematical models used to investigate the vibrations for each mode are presented. The excitation mechanisms and damping models are described in detail with respect to their significance for proper modeling. The input shaping method and variable pitch cutter concepts and their effects on suppressing vibrations of various mechanical systems are also described.

In the second section, the challenges encountered with the rotary cone bit's bearing and seal while drilling are briefly addressed. Suggested improvements to improve the bearings and seals for longer operations are outlined. Innovative designs for the lubrication system are also presented.

2.2 Drillstring Vibrations

2.2.1 Introduction

Vibrations have been reported to have a major effect on drilling performance. Vibrations can affect weight on bit (WOB), rate of penetration (ROP), and drilling direction and can also cause severe damage to drilling tools, such as bottomhole assemblies (BHA), measurement while drilling (MWD) tools, cutters, and bearings. Additionally, they can reduce the efficiency of the drilling process by absorbing some of the total energy transmitted downhole.

Three types of vibrations have been observed while drilling. Lateral vibrations are dissipated due to contact with the borehole wall and can only be measured by means of special tools downhole. Torsional vibrations affect the torque applied by the rotary motor and can be measured in terms of the torque's fluctuations. Axial vibrations can be observed uphole by motion of the upper parts of the drillstring.

These three types of vibrations have been studied extensively for many years, both experimentally and mathematically. Mathematical models and computational calculations have been very useful in clarifying different characteristics of these vibrations, as well as in predicting responses to specified inputs. In the following sections a brief explanation is provided detailing the three modes of vibrations of drillstrings.

2.2.2 Lateral Vibrations

Lateral vibrations can cause enlargement of the borehole wall, as well as deviation of the drilling direction. The lateral vibrations of drillstrings have been recognized as the main cause of bottomhole assembly (BHA) failures. The BHA is the lowest part of a drillstring and consists of the collars, stabilizers, and downhole tools to which the drill bit is connected. Although lateral vibrations have major effects on performance of a drillstring, they were not studied for many years because they are not visible uphole. The development of downhole measurement tools has enabled the investigation of lateral vibrations and revealed the importance of these vibrations and their effect on downhole tools failures. Figure 2-1 illustrates lateral vibrations of drillstrings.

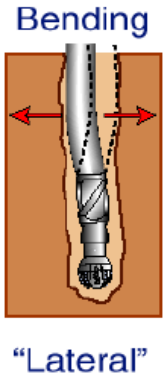

Figure 2-1: Lateral vibrations of drillstrings (Ashley et al., 2001)

Mathematical models have an important role in the investigation of lateral vibrations of drillstrings; both closed form solutions and the finite element discretization have been used to study these vibrations. Using the mathematical models, different aspects of drillstring behavior related to lateral vibrations have been studied. These studies have addressed natural frequency determination (Chen et al., 1995; Christofforou et al., 1997; Frohrib et al., 1967), critical bending stresses (Spanos et al., 1997), and lateral displacements prediction of drilling assemblies (Dykstra, 1996). In addition, Chevallier (2000) and Spanos et al. (2002) have provided preliminary results for nonlinear stochastic drill-string dynamics.

Damping has been applied to the models in different ways. Paslay et al. (1992) used an undamped model in their analyses, while Christoforou et al. (1997) used hydrodynamic damping due to the presence of the drilling mud. Spanos et al. (1997) used an expression for damping as a function of the vibration frequency and mud density. Dykstra (1996) also divided the damping matrix into two dissipative and non-dissipative matrices to take into consideration both Rayleigh damping and gyroscopic effects. Finally Spanos et al. (2002) used an extended Rayleigh damping in their model.

Some modifications have been made in the models to account for effects of some other features. Axial loading has been considered in various publications (Christofforou et al., 1997; Spanos et al., 1997; Spanos et al., 2002; Palsay et al., 1992). The drilling mud has usually been treated as an added mass (Chen et al., 1995; Spanos et al., 1997; Chevallier 2000), while it is sometimes considered for its damping effect (Christofforou et al., 1997). Contact with the borehole wall is another major area that caught attention (Christofforou et al., 1997; Spanos et al., 2002), while some other effects like gyroscopic moments are also included in some models (Chen et al., 1995; Christofforou et al., 1997). Figure 2-2 shows a model used by Spanos, Chevallier, and Politis (2002) to study nonlinear vibrations of drillstrings.

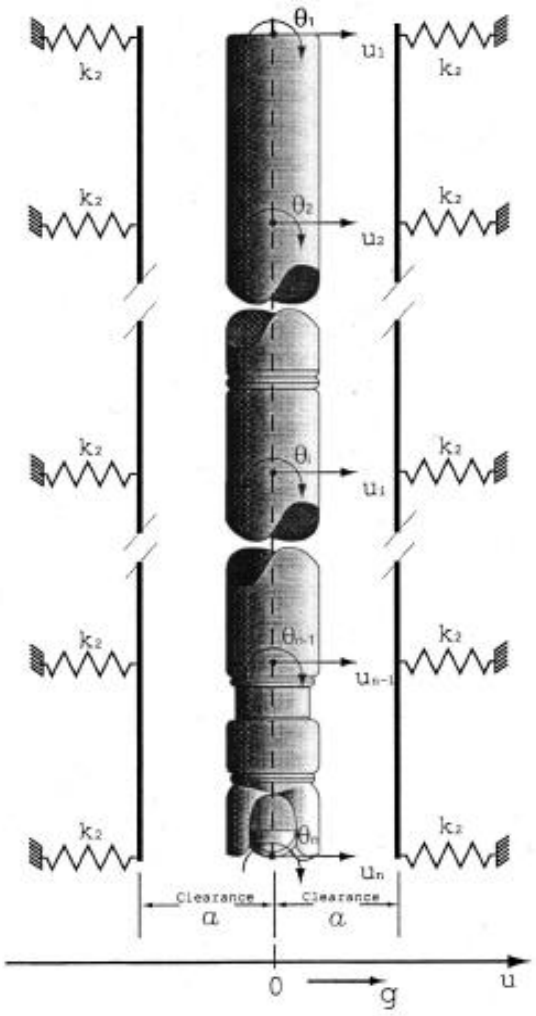

Figure 2-2: Nonlinear Lateral Vibrations Model (Spanos et al., 2002)

Different models of excitation, which causes lateral vibrations of drillstrings, have been proposed in the literature. Besaisow and Payne (1988) identified some of the sources for the excitations, such as bit

forces, drill collar mass imbalance, stabilizer loads, and drill pipe kinematics. Spanos et al. (1997) considered a monochromatic harmonic excitation for the drillstring system and modeled the lateral excitations induced by roller cone bits as a band limited white noise (2002). For those excitations induced by PDC bits, Spanos et al. (2002) considered the output result by passing the white noise through a second order filter, as shown in Figure 2-3.

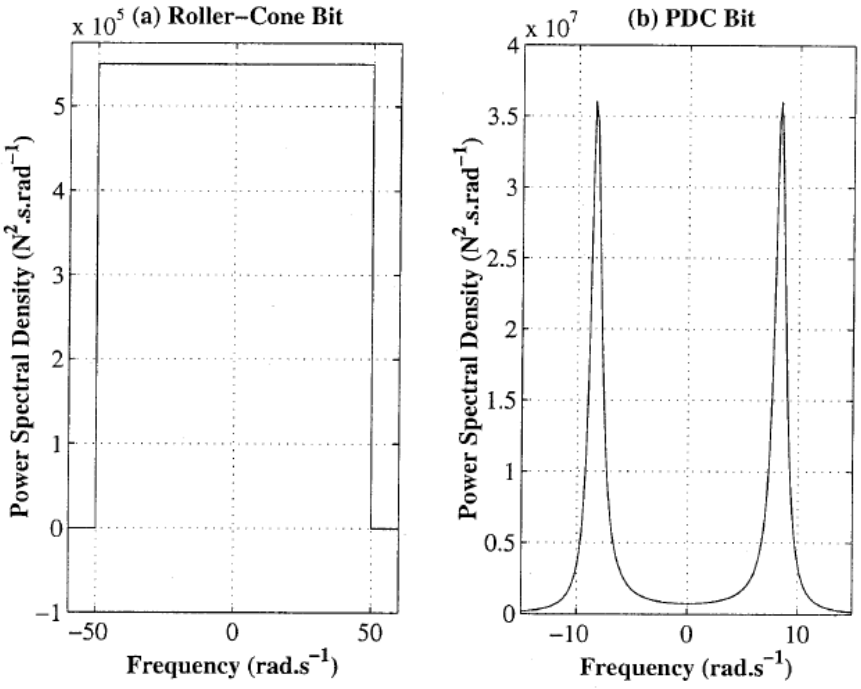

Figure 2-3: Excitation models for lateral vibrations for roller cone and PDC bits (Spanos et al., 2002)

2.2.3 Torsional Vibrations

Torsional vibrations of drillstrings are not seen uphole due to the fact that the rotary table in the surface acts as a clamp and attenuates most of the vibrations. MWD devices have assisted researchers in obtaining a better understanding of this type of drillstring vibrations and their effect on downhole tools and drilling performance. It has been stated that torsional vibrations can lead to excessive loading, resulting in equipment wear, joint failure, and damage to the drill bit (Brett, 1992; Elsayed et al., 1997). Figure 2-4 depicts these vibrations and a phenomenon called stick-slip motion which is caused by them:

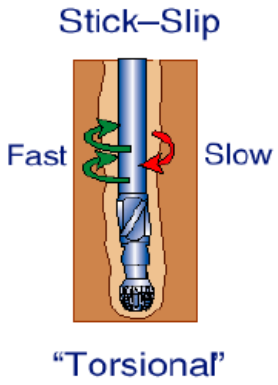

Figure 2-4: Torsional vibrations and "stick-slip" phenomenon (Ashley et al., 2001)

A variety of models have been used to study torsional vibrations of drillstrings. The main model which has been widely used for many years uses a torsional pendulum. In torsional pendulum model, drill pipes are considered as an inertialess spring connected to a mass which represents the bottomhole assembly (Dawson et al., 1987; Lin et al., 1991). Modifications have been made to adopt this model for further investigations; for example, the rotary table has been considered as another mass (Zamanian et al., 2007; Abbassian et al., 1998; Serrarens et al., 1998; Jansen et al., 1995), and coupling with other modes of vibration has also been considered, e.g., axial vibrations (Zamanian et al., 2007; Richard et al., 2007) or lateral vibrations (Abbassian et al., 1998; Leine et al., 2002). In most of the mentioned studies, viscous damping has been applied as a damping effect between the masses and the borehole wall (Serrarens et al., 1998; Jansen et al., 1995; Lin et al., 1991; Dawson et al., 1987). Figure 2-5 shows one of the mentioned models used by Jansen (1995) to study torsional vibrations of a sample drillstring.

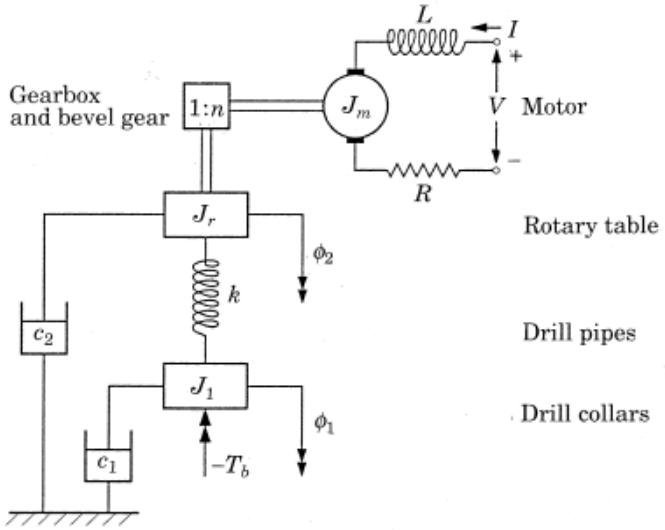

Figure 2-5: Model of drillstring for torsional vibrations (Jansen et al., 1995)

Choosing appropriate boundary conditions is another important step in the modeling of torsional vibrations of drillstrings. The upper node represents the rotary table and a constant rotary speed has been considered in some investigations for this point (Dawson et al., 1987; Leine et al., 2002; Richard et al., 2007; Serrarens et al., 1998; Jansen et al., 1995). In some cases a control relationship between the rotary table torque and the rotary speed has been considered in order to maintain desired rotary speed (Brett, 1992).

Modeling the excitation at the bit/rock interface is one of the most important issues in the study of torsional vibrations of drillstrings. Most models have implemented the dry friction concept to define the force or torque acting at the bottom of the drillstring, while all models relate the force or torque to the rotary speed of the drillstring. Dawson et al. (1987) used a linear piecewise model for the force and the rotary speed relation, while Lin et al. (1991) presented another model using a continuous exponential form. The torque at the bottom of the drillstring has also been defined in terms of a rational relation with the rotary speed (Leine et al., 2002) or as a nonlinear function to represent the combined torque on bit and frictional forces along the collars (Jansen et al., 1995), as shown in Figure 2-6.

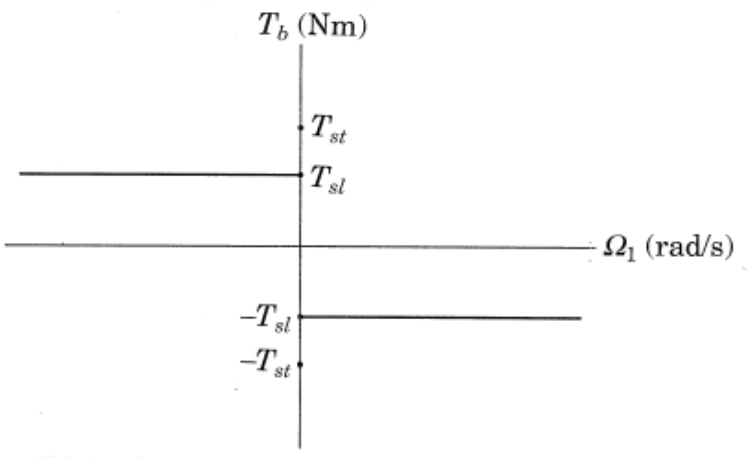

Figure 2-6: Torsional excitation model (Jansen et al., 1995)

2.2.4 Axial Vibrations

Axial vibrations can reduce the penetration rate of drilling due to fluctuations in weight on bit (WOB). These fluctuations are caused by the temporary lift-off of the drill bit from the formation, known as the "bit bounce" phenomenon, as shown in Figure 2-7. Axial vibrations can cause severe damage to sections of the drillstring, particularly the drill bit, and can significantly reduce the lifetime of the bit's bearings as a result of these fluctuations.

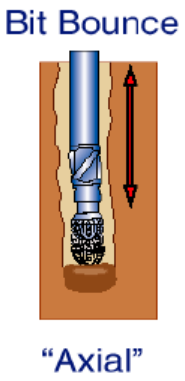

Figure 2-7: Axial vibration and "bit bounce" phenomenon (Ashley et al., 2001)

A variety of models have been used to investigate these vibrations. Continuous models were used in early studies to model drillstrings (Bailey et al., 1960; Paslay et al., 1963; Dareing 1968; Kreisle et al., 1970), while more recently, finite element models have been applied to axial vibration investigations (Spanos et al., 1995). Some studies, however, have not used a complete model for drillstrings, but have focused only on natural frequencies i.e. (Dareing, 1984). Figure 2-8 shows one of the models used in the literature to study axial vibrations of drillstrings.

Figure 2-8: Drillstring model for axial vibrations (Spanos, et al., 1995)

Implementation of damping into models is an important aspect of the studies of axial vibrations. Some investigations did not consider any type of damping, e.g. Bailey et al. (1960), while some others incorporated damping mechanisms into their models (Paslay et al., 1963; Dareing 1968; Kreisle et al.,

1970; Spanos et al., 1995). The two most common types of damping used include: simple viscous damping (Paslay et al., 1963; Kreisle et al., 1970), and frequency-dependent damping (Spanos et al., 1995).

Over the years, a great deal of research has been completed to investigate the effects of different parts of the drillstring on its axial vibrations, for example Kreisle et al. (1970) showed the importance of a shock sub in reducing axial vibrations and Dareing (1984) revealed the dominant effect of drill collar length on axial and torsional vibrations of drillstrings.

In order to reach a better prediction of drillstring axial vibrations, it is important to model the excitations accurately. This subject, therefore, has been one of the main areas of investigation of drillstring vibrations. Dareing (1984) identified various sources of excitation, such as pump pressure, sidewall friction, and drill bit/formation interaction. He also indicated that the various types of drill bits (i.e., roller cone, diamond, PDC) generate different loading conditions to the bottom end of the drillstring. A harmonic excitation is the main mechanism used in previous studies of drilling with roller cone bits. This harmonic excitation has been expressed in terms of sinusoidal motion, which is applied at the bit (Dareing, 1968). Due to the rolling of the bit, a multi-lobed surface is formed on the formation; the number of lobes formed depends on the number of cones on the bit. This lobed-pattern can be defined by a profile with sinusoidal angular variation elevation (Spanos et al., 1995), as shown in Figure 2-9:

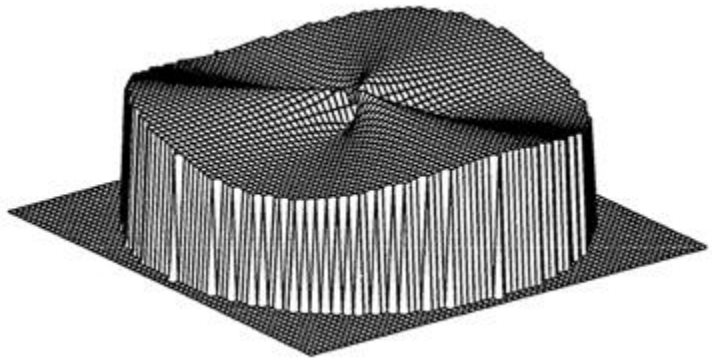

Figure 2-9: Multi-lobed surface of a formation (Spanos et al., 1995)

2.2.5 Damping

To illustrate the importance of taking damping into consideration to predict the drillstring vibrational behavior, it is necessary to describe this concept in more detail. Different approaches have been used to implement damping in modeling of drillstring vibrations. One of these methods is Rayleigh damping

which has been widely used in various analyses e.g., (Dykstra, 1996; Chevallier, 2000). In this method, the damping matrix, C, is assumed to be a linear combination of the system mass, M, and stiffness, K, matrices:

$$C = \alpha M + \beta K \tag{2-1}$$

One of the major advantages of the Rayleigh method is that the damping matrix reduces to a diagonal form in the principal coordinates, which is particularly useful for the mode superposition method. It is possible to use matrices other than the mass and the stiffness matrices for the Rayleigh method; any matrix possessing the free vibration mode shape orthogonality property may be used. This form of damping, which is known as the extended Rayleigh damping, has also been used (Spanos et al., 2002).

While the coefficients α and β should be determined for two specific modes, this method may not model the damping for higher modes accurately. To address this problem, another approach has also been proposed (Spanos et al., 1997; Payne, 1992), in which the critical modal damping ratio is expressed as:

$$\zeta = af^b \tag{2-2}$$

where f represents the natural frequency in *Hz* and a and b are coefficients dependent on the drilling mud density.

A simpler method to implement the Rayleigh damping is to consider an identical damping ratio for all modes. Although this method is not as accurate as the aforementioned models, it can be useful in clarifying various aspects of the vibrational behavior of a system e.g., (Chevallier, 2000; Payne, 1992). It should also be stated that the span of published damping ratios which range from 1% to 65%, depends on the well condition and added lubricants (Brakel, 1986).

2.2.6 Input Shaping Method for Reducing Vibrations

The shaping method involves the convolution of a desired input with a sequence of impulses to produce an input function that reduces vibration. Impulse amplitude and timing are the parameters that dictate the performance of the system. This method is applicable for systems with single-mode or multi-modes of vibrations and can be used for single-input or multi-input systems. The input shaping method has been used in a wide range of applications due to the ease of implementation and robustness to parameter uncertainty. Varying aspects of this method and its applications have been described in different publications (Singer et al., 1990; Singer et al., 1990; Singer et al., 1997; Singhose et al., 1990; Pao 1999; Pao et al., 1995; Tzes et al., 1993). Figure 2-10 shows the steps of convolving an input using input shapers.

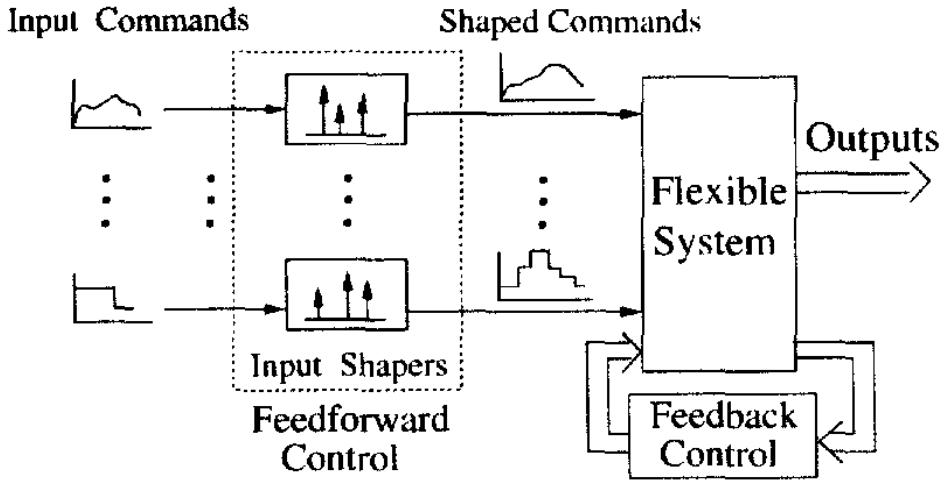

Figure 2-10: Steps of convolving an input using input shapers (Pao, 1999)

Figure 2-11 shows the effect of the input shapers on the final response of the system, illustrating how they eliminate or reduce the vibrations of the systems.

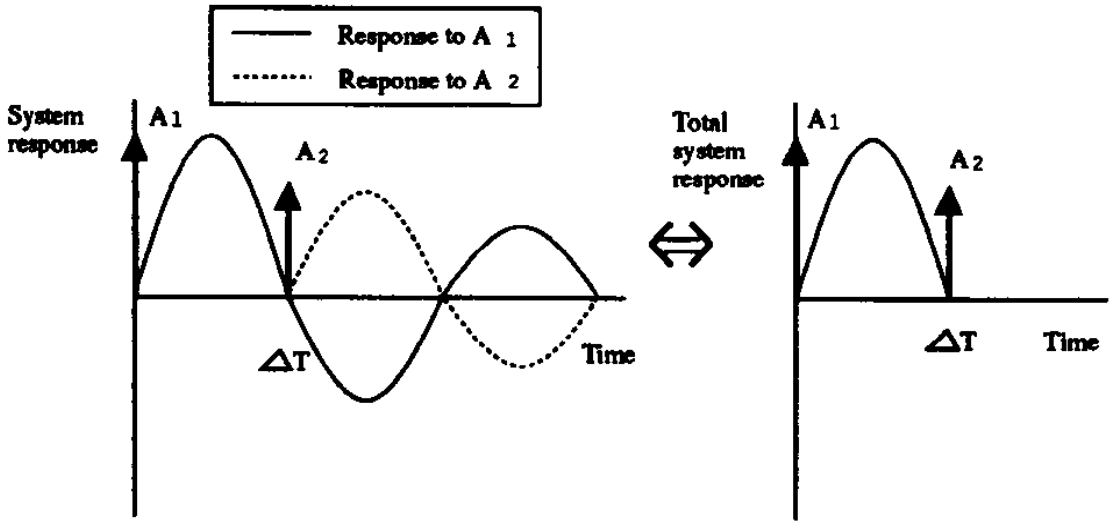

Figure 2-11: Effect of the input shapers on the final response of the system (Singhose et al., 1990)

As an example, Figure 2-12 shows the endpoint position for a flexible robotic manipulator (link) for both unshaped and shaped inputs, where vibrations have been reduced dramatically for the shaped input.

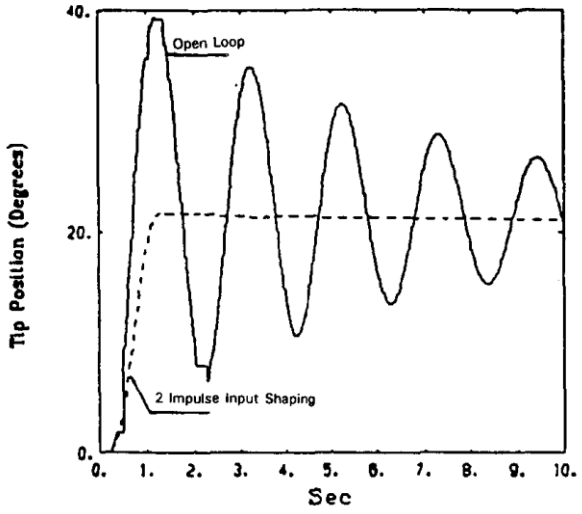

Figure 2-12: Endpoint position of a flexible robotic link before and after shaping inputs (Tzes et al., 1993)

2.2.7 Using Variable Pitch Cutters to Increase Stability in Milling

Chatter vibrations are a major problem in milling and can result in reduced productivity, decreased cutting-tool life, poor surface finish, and high material removal rates. Different approaches have been identified to overcome this problem, as described by Altintas et al. (1999); however, none of the current approaches can solve the problem completely.

The use of variable pitch milling cutters was first proposed by Slavicek (1965) to address this problem and has been investigated and further developed in subsequent studies. The main concept of this idea is to use an irregular pattern for cutters. Different investigations have shown that this method results in the reduction of the chatter vibrations and dimensional surface error and an increase in the stability of the milling cutters (Altintas et al., 1999; Shirase et al., 1996). Figure 2-13 shows the difference between constant pitch and variable pitch milling cutters.

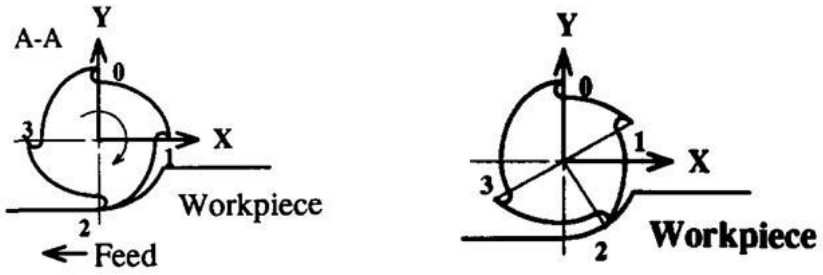

Figure 2-13: Constant-pitch cutters (left) versus variable pitch cutters (right) (Shirase et al., 1996)

2.3 Rotary Drill Bit's Bearing and Seal Designs

2.3.1 Introduction

Failure of bearings is one of the main causes of damage to drill bits. Hard formations and system vibrations may generate elevated forces and shocks resulting in damage to the bearings. The presence of drilling mud and the rock chips produced while drilling requires that the bearings be sealed off from their external environment; however, these seals often have problems maintaining their effectiveness. Higher temperature can affect both the bearing's and seal's performance and reduce their lifetime. High temperatures are generated by the friction of the bearing surfaces; for very deep wells the high temperature of the earth also adds to the overall bit's temperature. Elevated pressure may also result in premature damage to the seal, allowing debris and drilling liquid to enter the bearing's cavity and prevent the bearings from proper functioning. This situation occurs most commonly in very deep wells, where the heavy drilling mud circulated through the drillstring can induce significant pressure on the seal's face.

There have been numerous attempts to address the aforementioned challenges. A variety of different designs and arrangements have been proposed to withstand the generated forces for extended durations. Attempts have been made to fabricate seals capable of withstanding higher pressures and higher temperatures. The configuration of the seals' components has also been revised to help them operate more consistently. Finally, innovative designs have been presented for a lubrication system to allow better performance of the bearings and seals. In the next section, these previous ideas are reviewed.

2.3.2 Literature Review

Typical roller cone bits use a combination of thrust and radial bearings to withstand external forces. Thrust bearings, which are located on the front head of the arm's shaft (Persson, 1981) can fail due to elevated thrust forces. One solution to overcome this problem is to use tapered roller bearings, which are able to withstand a combination of radial and axial forces. Olschewski et al. (1983) used a combination of tapered and cylindrical roller bearings, as shown in Figure 2-14. Some designs have also used partially-tapered cylindrical rollers to include such an effect (Levefelt, 1980; Villaloboz, 1977).

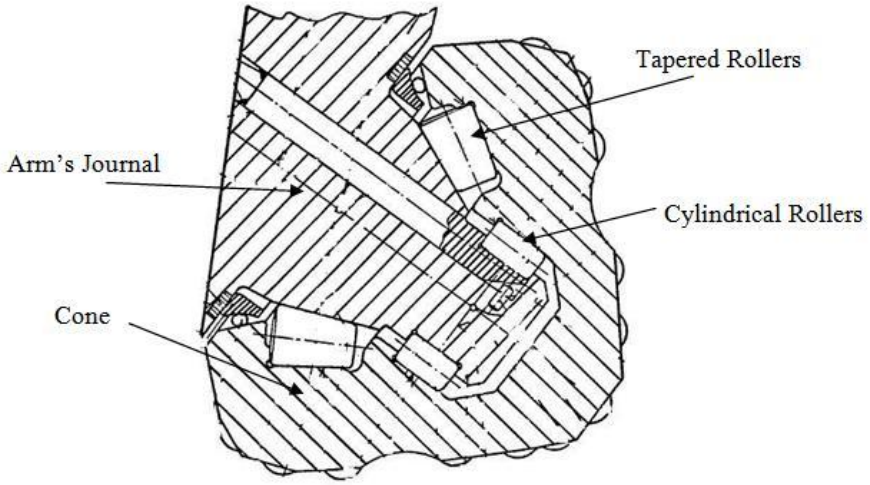

Figure 2-14: Tapered and cylindrical roller bearings (Olschewski et al., 1983)

The bearings must be sealed off from the debris and the drilling mud outside. While the sealing package consists of different parts, the configuration of these parts has been another important area of research towards improving sealing performance. Simple o-rings were used as the early seals for rotary cones, but metal seals and energizers are now used as well. In one configuration, two metal seals face each other while energizers push them together. This configuration was modified to replace one of the metal seals with the cone seal insert, as well as an excluder seal to prevent debris from entering the cone cavity and keep the energizer from rotating (Lin 2006; Nguyen 2006; Zahradnik et al., 2000), as shown in Figure 2-15. In some cases, a dynamic seal made of a relatively softer material has also been added between two metal seals (Yong et al., 2006). The use of two elastomeric seals back to back is another proposed method known as dual-seal method (Portwood et al., 2004; Mourik et al., 2004).

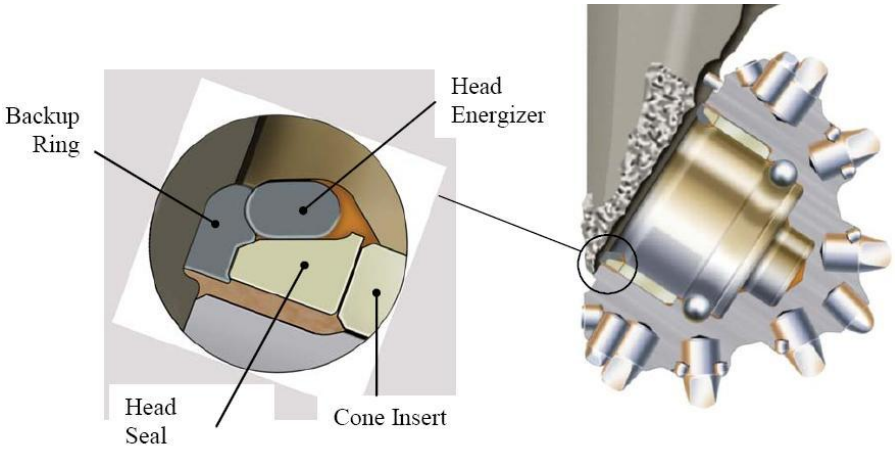

Figure 2-15: The sealing package (Grimes et al., 2006)

Other means have also been employed to help seal the cones. In some cases, eccentric seal cavity has been used to agitate the fluid and avoid mud packing (Nguyen, 2006). Other applications have used a mud diverter installed on the bit leg and the back face of the cone to divert debris from the seal gland area. (Lin, 2006), as shown in Figure 2-16. Debris diversion can be performed by means of a gage scraper as well (Nguyen et al., 2006).

Figure 2-16: Mud diverter (Baker Hughes)

Some publications presented the effects of some of the prescribed designs and their advantages and disadvantages for actual field tests (Mcleod et al., 2000; Carre et al., 2001; Grimes et al., 2006; Urbieta et al., 2006).

The cone must be retained on the arm while being able to rotate which demands a special retaining method. A common method involves the insertion of ball bearings through a specific hole in the arm; the balls keep the cone in the place as well as allowing it to rotate as shown in Figure 2-17. Although applicable, this method increases the number of elements used for manufacturing. Attempts to simplify this holding method include the use of a retainer ring (Morris, 1979), or the use of cylindrical rollers to hold the cone on the shaft (Karlsson, 2001).

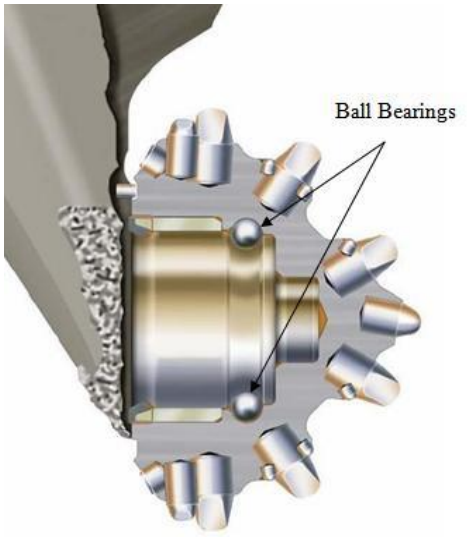

Figure 2-17: Ball bearings for retaining the cone (Urbieta et al., 2006)

An effective lubricating system is of great importance to maintaining the consistent performance of the bit's bearings. In mine drilling; some grease is used to cover the bearing surfaces as well as cooling by air flow. For oil drilling, a lubrication system usually comprises a reservoir, a pressure compensator, and passageways as shown in Figure 2-18.

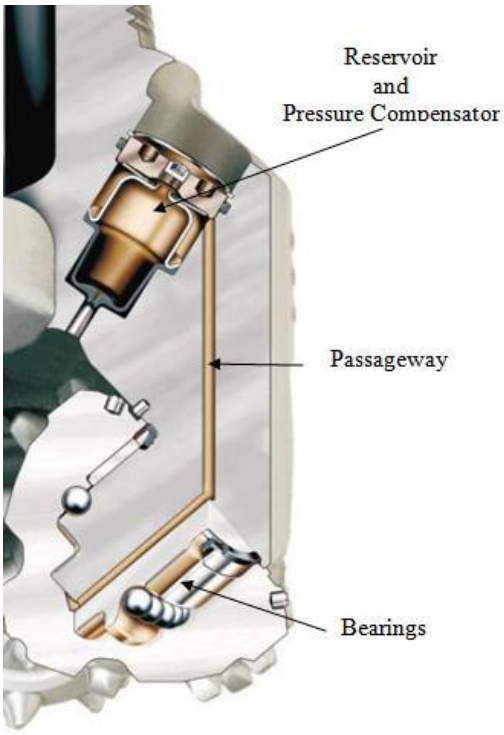

Figure 2-18: Lubrication system for rotary cone bits (Baker Hughes)

Modifications of different parts of the lubricating system have been made to improve the lubricating action. For example, researchers have attempted several methods for generating a pumping action to circulate lubricant throughout the passageways; these methods include using the pressure difference generated inside the cone's cavity while drilling (Dick et al., 2006), employing a plunger action provided by fluid flow (Rives, 2007), and inducing pumping forces by adding features to the inside cavity of the cone, such as grooves and ramp surfaces formed on the trust bearing surface (Hooper, 1993; Keller et al., 1980; McQueen, 1979) , gerotor pump elements (Hixon, 1992), and screw pump elements (Walters, 1980). Another area of study has included control of the direction of the lubricant's flow through passageways; for example, by adding valves (Daly, 1984) or changing the geometry of the passageways to induce resistance in the desired directions (Phelan, 1983). Finally, some designs have been presented on the reservoir and pressure compensator devices to provide the reservoir with better protection by changing its location (Slaughter et al., 2001) and adding a relief valve to the elastomeric member used as the compensator (Delgado et al., 1991).

Chapter 3

Mathematical Basics of Drillstring Vibration Modeling and Analysis

3.1 Outline

In this chapter, the beam element stiffness and mass matrices for each mode of drillstring vibrations are presented. The responses of single-degree and multi-degree of freedom systems to an impulse are described. For a multi-degree of freedom system, two different approaches, modal analysis and state-space formulation, are reviewed.

3.2 Beam Element Stiffness and Mass Matrices

A beam element is shown in Figure 3-1 with two nodes and their assigned degrees of freedom. To model a drillstring, one can assemble these elements to represent the entire system. Different pairs of degrees of freedom can be selected to study different modes of vibrations. Element stiffness and mass matrices are presented here, which can be used for different modes of vibrations.

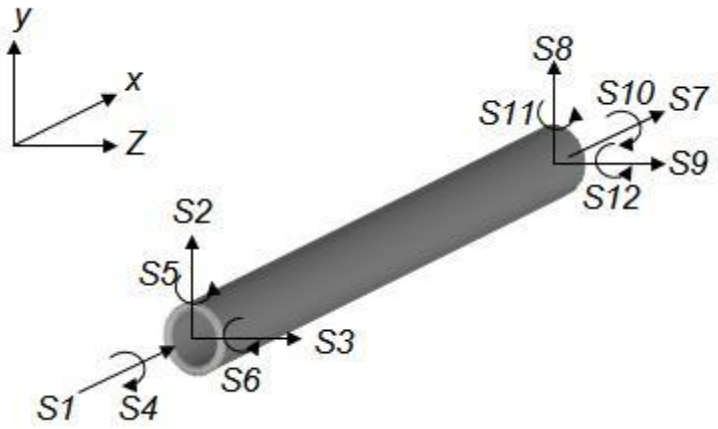

Figure 3-1: The beam element and its 12 degrees of freedom

3.3 Lateral Vibrations

For lateral vibrations, we follow the assumptions made by Chevallier (2000), who used the shearing forces S_2 and S_8, and the bending moments, S_6 and S_{12}, to study the lateral vibrations. Chevallier modified the basic equations to account for the effect of the axial load; he assumed a constant axial force and applied the technique described by Przemieniecki (1968). He revealed that this load permits the consideration of the WOB and results in a decrease of the natural frequencies for compressible loads, and

a "stiffening" of the string for the tensile loads as stated in (Dareing, 1984; Spanos et al., 1997). The axial load, P, is considered positive if it is tensile. The final expression for the stiffness matrix derived by Chevallier has the form:

$$K = \begin{bmatrix} \frac{12EI_z}{{l_e}^3} + \frac{6P}{5l_e} & \frac{6EI_z}{{l_e}^2} + \frac{P}{10} & \frac{-12EI_z}{{l_e}^3} - \frac{6P}{5l_e} & \frac{6EI_z}{{l_e}^2} + \frac{P}{10} \\ \frac{6EI_z}{{l_e}^2} + \frac{P}{10} & \frac{4EI_z}{l_e} + \frac{2Pl_e}{15} & \frac{-6EI_z}{{l_e}^2} - \frac{P}{10} & \frac{2EI_z}{l_e} - \frac{Pl_e}{30} \\ \frac{-12EI_z}{{l_e}^3} - \frac{6P}{5l_e} & \frac{-6EI_z}{{l_e}^2} - \frac{P}{10} & \frac{12EI_z}{{l_e}^3} + \frac{6P}{5l_e} & \frac{-6EI_z}{{l_e}^2} - \frac{P}{10} \\ \frac{6EI_z}{{l_e}^2} + \frac{P}{10} & \frac{2EI_z}{l_e} - \frac{Pl_e}{30} & \frac{-6EI_z}{{l_e}^2} - \frac{P}{10} & \frac{4EI_z}{l_e} + \frac{2Pl_e}{15} \end{bmatrix} \quad (3\text{-}1)$$

In this equation, E is the Young's modulus of the material that constitutes the elements, I_z is the moment of inertia with respect to the z-axis and l_e is the length of the element, as shown in Figure 3-1.

The mass matrix considered by Chevallier to represent the BHA mass takes into consideration the added mass effects due to the presence of the drilling mud inside and outside of the drillstring, as has also been used in Spanos et al. (1997). The final expression for the mass matrix is:

$$m_e = \begin{bmatrix} \frac{13M_t}{35} + \frac{6\rho I_z}{5l_e} & \frac{11M_t l_e}{210} + \frac{\rho I_z}{10} & \frac{9M_t}{70} - \frac{6\rho I_z}{5l_e} & \frac{-13M_t l_e}{420} + \frac{\rho I_z}{10} \\ \frac{11M_t l_e}{210} + \frac{\rho I_z}{10} & \frac{M_t {l_e}^2}{105} + \frac{2\rho I_z l_e}{15} & \frac{13M_t l_e}{420} - \frac{\rho I_z}{10} & \frac{-M_t {l_e}^2}{140} - \frac{\rho I_z l_e}{30} \\ \frac{9M_t}{70} - \frac{6\rho I_z}{5l_e} & \frac{13M_t l_e}{420} - \frac{\rho I_z}{10} & \frac{13M_t}{35} + \frac{6\rho I_z}{5l_e} & \frac{-11M_t l_e}{210} - \frac{\rho I_z}{10} \\ \frac{-13M_t l_e}{420} + \frac{\rho I_z}{10} & \frac{-M_t {l_e}^2}{140} - \frac{\rho I_z l_e}{30} & \frac{-11M_t l_e}{210} - \frac{\rho I_z}{10} & \frac{M_t {l_e}^2}{105} + \frac{2\rho I_z l_e}{15} \end{bmatrix} \quad (3\text{-}2)$$

In this equation, ρ and M_t are the density and the total mass of the element, respectively. The total mass of the element results from the mass of the element itself, as well as the added mass of the drilling fluid inside the tubular, M_i, and in the annulus, M_o. Chevallier also used a technique first proposed by Chen (1995) to account for fluid added-mass when a rod is vibrating inside a cylinder. The approach accounts for a constant parameter, C_m, which multiplies the mass of displaced fluid between the drilling assembly and the borehole, as follows:

$$M_t = M + M_i + C_m M_o \quad (3\text{-}3)$$

The coefficient C_m is a function of the radii of the bore hole and the drill string, the circular frequency of displacement, and the kinematic velocity of the drilling mud.

3.4 Torsional Vibrations

For torsional vibrations, the twisting moments S_4 and S_{10} are used to form the element stiffness matrix. The element stiffness matrix can then be defined as stated by (Przemieinecki, 1968):

$$k_e = \frac{GJ}{l}\begin{bmatrix} 1 & -1 \\ -1 & 1 \end{bmatrix} \tag{3-4}$$

In this formula, *G* is the shear modulus, *l* is the length of the element, and *J* is the area moment of inertia, as defined below:

$$J = \frac{\pi}{2}\left(r_o^4 - r_i^4\right) \tag{3-5}$$

In this formula, r_o and r_i are the outer and inner diameter of the pipe, respectively.

The element mass matrix also is described by (Przemieinecki, 1968) as follow:

$$m_e = \frac{\rho J_x l}{6}\begin{bmatrix} 2 & 1 \\ 1 & 2 \end{bmatrix} \tag{3-6}$$

where J_x is the polar moment of inertia, which is equal to J in equation (3-5) for circular cross sections.

3.5 Axial Vibrations

For axial vibrations, the axial forces S_1 and S_7 are used to form the element stiffness matrix. The element stiffness matrix can then be defined as stated by (Przemieinecki, 1968):

$$k_e = \frac{EA}{l}\begin{bmatrix} 1 & -1 \\ -1 & 1 \end{bmatrix} \tag{3-7}$$

In this expression, *E* is the Young's modulus, *l* is the length of the element, and *A* is the cross section of the element.

The element mass matrix also is described by Przemieinecki (1968) as shown below:

$$m_e = \frac{\rho A l}{6}\begin{bmatrix} 2 & 1 \\ 1 & 2 \end{bmatrix} \tag{3-8}$$

These element matrices are later assembled to model the entire drillstring for different modes of vibrations.

3.6 Response to an Impulse Input

In this section, a brief review of the response of single-degree and multi-degree of freedom systems to an impulsive input is presented. Two approaches, including modal analysis and state-space formulation, for finding the response of multi degree of freedom systems are described. Calculations for determining the total energy of the system for both methods are provided as well, to present a measure for improving vibrational behavior of the system.

3.6.1 Single-Degree of Freedom System

For a single-degree of freedom system, the equation of motion for an impulse input can be expressed as:

$$m\ddot{x} + c\dot{x} + kx = f\delta(t) \tag{3-9}$$

Where *m*, *c*, and *k* are the mass, damping, and stiffness of the system, respectively, f is the amplitude of the impulse and $\delta(t)$ is the Dirac delta function.

For such a system, the response can be determined as (Rao, 2004):

$$x(t) = \frac{fe^{-\zeta\omega_n t}}{m\omega_d} sin\,\omega_d t \tag{3-10}$$

In this formula, f, ζ, ω_n and *m* are the amplitude of the impulse, damping ratio of the system, natural frequency and mass, respectively. Figure 3-2 shows the impulse response for a typical single-degree of freedom system.

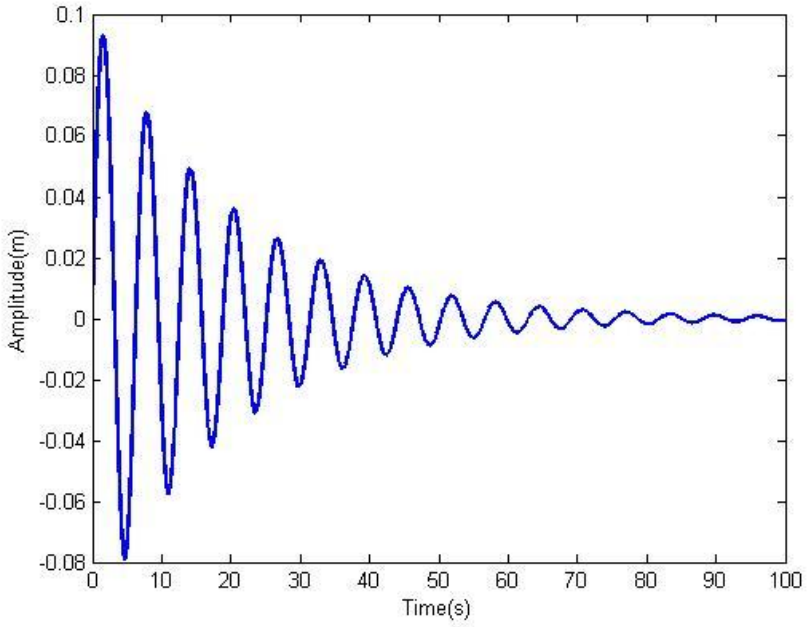

Figure 3-2: Impulse response for a typical mechanical system

3.6.2 Multidegree of Freedom System

For a multi-degree of freedom system, the equation of motion for an impulse input can be expressed as follows:

$$M\ddot{\boldsymbol{x}} + C\dot{\boldsymbol{x}} + K\boldsymbol{x} = \boldsymbol{F}\delta(t) \tag{3-11}$$

In this formula, *M*, *C*, and *K* are the mass, damping, and stiffness matrices, respectively, while $\boldsymbol{x}$ and $\boldsymbol{F}$ represent the displacement and force vectors, respectively.

One approach to finding the impulse response for a multi-degree of freedom system is to use a modal matrix and generalized coordinates. Using these two components allows the decoupling of equations and

determining the response for each degree of freedom. Furthermore, a modal superposition method can be used to determine the displacement vector, as follows:

$$\boldsymbol{x}(t) = X\boldsymbol{q}(t) \tag{3-12}$$

In this formula X is the modal matrix and $\boldsymbol{q}$ is the generalized coordinate vector.

Rewriting the equation of motion for generalized coordinates results in the following equation:

$$M^{'}\ddot{\boldsymbol{q}} + C^{'}\dot{\boldsymbol{q}} + K^{'}\boldsymbol{q} = \boldsymbol{Q}\delta(t) \tag{3-13}$$

While $M^{'}$, $C^{'}$, and $K^{'}$ are the generalized mass, damping, and stiffness matrices, respectively. These matrices are defined as:

$$M^{'} = X^{T}MX \tag{3-14}$$

$$C^{'} = X^{T}CX \tag{3-15}$$

$$K^{'} = X^{T}KX \tag{3-16}$$

$\boldsymbol{Q}$ is the generalized force vector, which is defined as:

$$\boldsymbol{Q} = X^{T}\boldsymbol{F} \tag{3-17}$$

In this case, the system equations can be described in terms of n single-degree of freedom systems, which can easily be solved for a specific input:

$$\ddot{q}_i(t) + 2\zeta_i\omega_i\dot{q}_i(t) + \omega_i^2 q_i(t) = \frac{Q_i\delta(t)}{M^{'}{}_i} \quad n = 1, \dots, n \tag{3-18}$$

in which n is the number of degrees of freedom, ζ_i is the i-th modal damping ratio, ω_i is the i-th natural frequency, Q_i is the i-th element of the vector of generalized force, and $M^{'}{}_i$ is the (i,i)-th component of the generalized mass matrix.

Now the response for each degree of freedom can be defined in a same manner as explained previously:

$$q_i(t) = \frac{Q_i e^{-\zeta_i\omega_{ni}t}}{M^{'}{}_i\omega_{di}} sin\,\omega_{di}t \tag{3-19}$$

Using this response, we are able to calculate the kinetic and potential energies for the entire system. Expressed in generalized coordinates, the kinetic and potential energies are:

$$KE = \frac{1}{2}\dot{q}^{T}M^{'}\dot{q} \tag{3-20}$$

$$PE = \frac{1}{2}q^{T}K^{'}q \tag{3-21}$$

The total energy of the system can be described as shown below:

$$E_T = KE + PE \tag{3-22}$$

Another approach to solve such an equation is to use state-space formulation. A typical state-space formulation can be expressed as:

$$\dot{X} = A_s X + B_s U \tag{3-23}$$

$$Y = C_s X + D_s U \tag{3-24}$$

where X is the state variable, U is the input and Y is the output.

Rewriting our system in state-space formulation results in:

$$X = \begin{bmatrix} x \\ \dot{x} \end{bmatrix} = \begin{bmatrix} X_1 \\ X_2 \end{bmatrix} \tag{3-25}$$

$$\dot{X} = \begin{bmatrix} \dot{x} \\ \ddot{x} \end{bmatrix} = \begin{bmatrix} X_2 \\ M^{-1}F\delta(t) - M^{-1}CX_2 - M^{-1}KX_1 \end{bmatrix} \tag{3-26}$$

$$\dot{X} = \begin{bmatrix} [0]_{n\times n} & I_{n\times n} \\ -M^{-1}K & -M^{-1}C \end{bmatrix} X + \begin{bmatrix} [0]_{n\times 1} \\ M^{-1}F \end{bmatrix} \delta(t) \tag{3-27}$$

The output can then be defined as:

$$\mathrm{Y} = \begin{bmatrix} x \\ \dot{x} \end{bmatrix} = IX \tag{3-28}$$

Finally, the kinetic and potential energies can be calculated directly using the displacement and velocity vectors:

$$KE = \frac{1}{2}\dot{x}^T M\dot{x} \tag{3-29}$$

$$PE = \frac{1}{2}x^T Kx \tag{3-30}$$

It should be noted that to use this method, the damping matrix C should be available at the beginning. In this case, the modal analysis and Rayleigh formulation can be used to derive the damping matrix, C which is required for the state-space formulation.

Chapter 4
Drillstring and Excitation Models

4.1 Outline

In this chapter, the finite element model used by Chevallier to study lateral vibrations of drillstring is reviewed. Based on this model, a new model is proposed that is capable being used to analyze all modes of vibrations of drillstrings. The general excitation model is also presented.

4.2 Introduction

The proposed general model presented in this thesis is based on the finite element model used by Chevallier (2000) to investigate lateral vibrations of drillstrings in a blasthole assembly. While blasthole drilling requires short length drillstrings, Chevallier's model can be used for the proposed model. The specifications outlined for drill pipe and drill collar elements can be directly transferred to the new model. Although Chevallier's model was used to study lateral vibrations, it can be used as an appropriate base for the study of other modes of vibrations. Therefore in this thesis Chevallier's model for lateral vibrations is modified and used as a base for the study of axial and torsional vibrations of the drillstring.

4.3 Finite Element Model of Drillstring for Lateral Vibrations (Chevallier, 2000)

Chevallier utilized a length of approximately 38 m for the bottomhole assembly (BHA), which consists of two stabilizers, drill pipes, and drill collar elements. Drill pipe elements constitute approximately one third of the total length of the assembly in his model, while the rest of elements are considered to be drill collars. In his assumption, drill pipe and drill collar elements possess identical material properties, element length, and internal diameters; therefore, only their external diameters differ. In addition it was assumed that drill collars are subject to a compressive force due to the WOB. Figure 4-1 shows the geometry of Chevallier's finite element model.

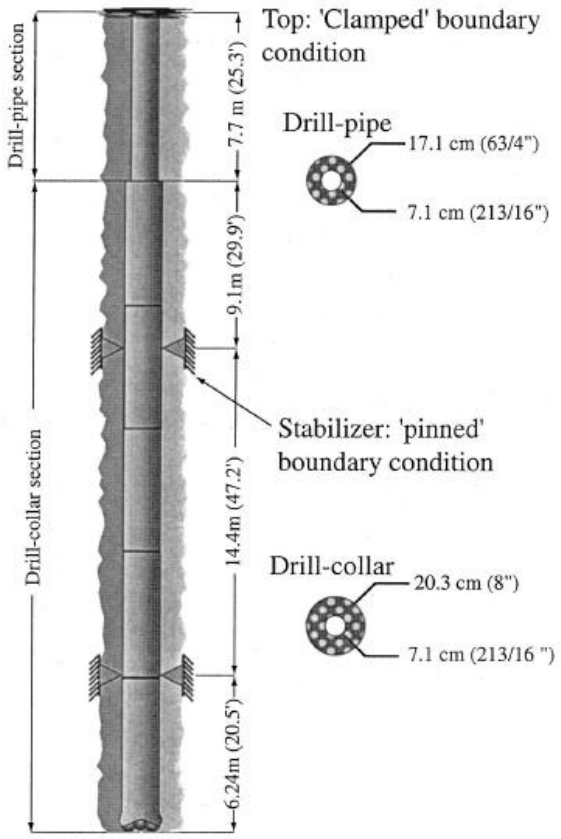

Figure 4-1: Drillstring Model by Spanos, Chevallier, and Politis (Spanos et al., 2002)

Table 4-1 shows the element properties for drill pipes and drill collars elements.

Table 4-1: Drill pipe and drill collar properties (Chevallier, 2000)

Specifications	Drill Pipes	Drill Collars
Number of pipe elements	16	64
Pipe element length	2.4 m	2.4 m
External diameter	17.1 cm	20.3 cm
Internal diameter	7.1 cm	7.1 cm
Density	7833 $Kg.m^{-3}$	7833 $Kg.m^{-3}$
Young modulus	207 GPa	207 GPa
Compressive force	0 N	10^4 N

Chevalier has applied specific boundary conditions to the BHA assembly: a "clamped" condition is assumed at the top, which restrains both the lateral displacement and the rotation of the first node. Stabilizers are located at distances 16.8 m (55') and 31.2 m (102.4') from the top of the model; these stabilizers are modeled with pinned boundary conditions so that the corresponding nodes are restrained in

their lateral displacement but are free to rotate. Finally, the bit is free of boundary conditions and is subjected to a lateral excitation force.

4.4 The New Finite Element Model

Chevallier's model is used as the base for the new model proposed in this thesis. Some minor changes have been made to adapt it for this study's objectives. In the new model, the entire drillstring consists of 16 elements, each of which has the same mass and stiffness matrices as the original model. In the original model proposed by Chevallier, 80 elements were used. In this study, it is assumed that these elements have identical properties, representing the drill collar properties. The effect of the added mass has not been considered in the new model and it has been assumed that there is no contact between the drillstring and the borehole wall.

Figure 4-2 shows the new model proposed in this thesis.

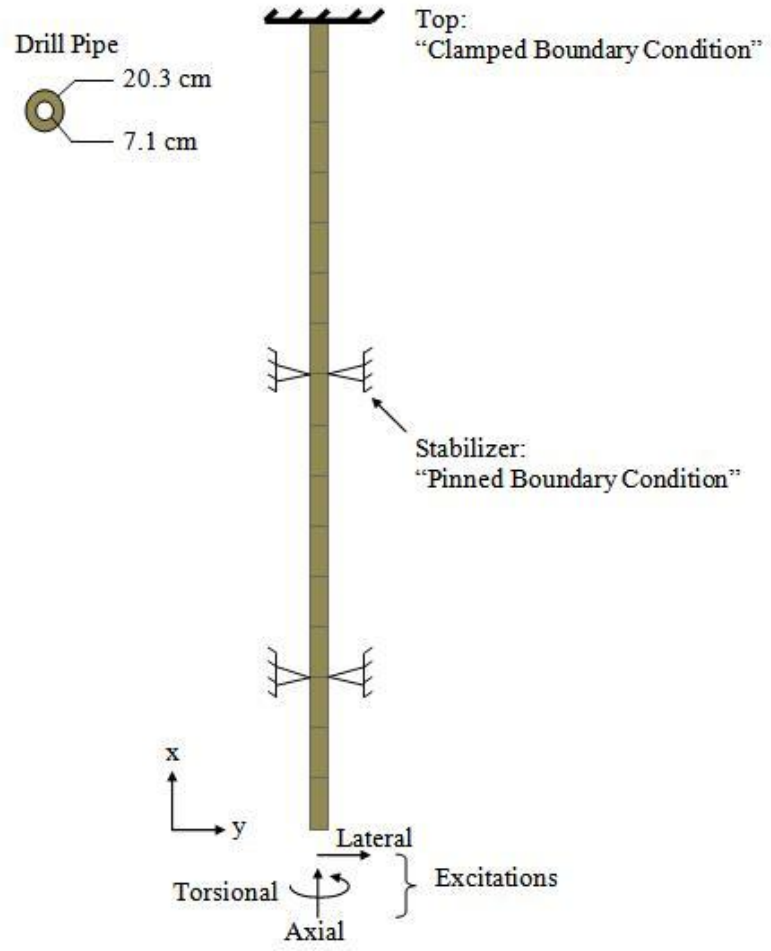

Figure 4-2: ledom gnirtsllird desoporP

It should be noted that the stabilizers only affect lateral vibrations of the drillstring; therefore, there is no restriction for axial and torsional modes. Each mode also has its own specific type of excitation, though all three types of excitations are shown in the model.

4.5 Excitation model

As discussed in the literature review, various excitation models have been used to investigate lateral vibrations of the drillstring. In this section, a new approach for the excitation mechanism while drilling with rotary cone bits is presented. In this case, the contact between an insert and the rock is modeled with an impulse, as shown in Figure 4-3.

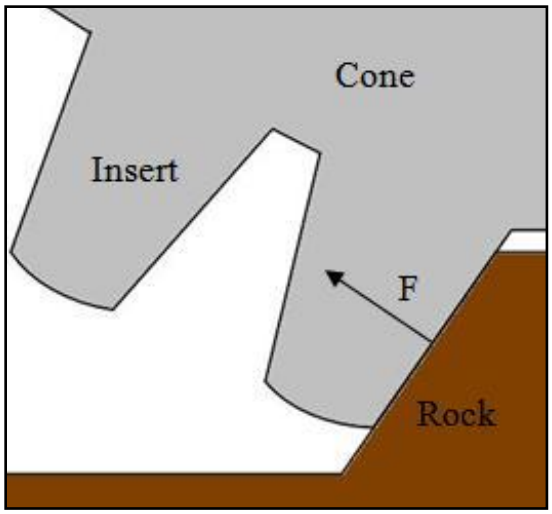

Figure 4-3: Cone-Rock interaction modeled as an impulse

A general coordinate can be defined, as shown Figure 4-4, such that one axis is towards the center of the drillstring, the other is parallel to the axis of the drillstring, and the final axis is perpendicular to the first two. The force induced in the contact area of the insert and the rock can be projected on this coordinate system. Three impulsive forces are generated while the insert hits the rock. The F_y component is considered as the source of excitation for lateral vibrations, F_x as the source of excitation for axial vibrations, and the torque induced by F_z as the source of excitation for torsional vibrations. Figure 4-4 illustrates these forces.

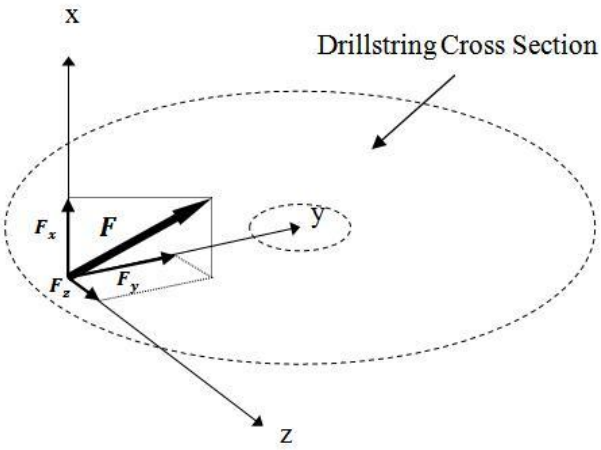

Figure 4-4: Proposed coordinate and impulsive force

While the cone rotates due to the rotation of the bit, a series of inserts hit the rock in sequence. Eventually a set of impulses are applied to the bit due to this rotation, resulting in a specific input pattern. This pattern can be characterized by two parameters: one representing the entire time of one rotation for a cone, and the other showing the time spacing between two sequential inserts, as shown in Figure 4-5. For simplicity, it is assumed that all impulses are identical and have a unity magnitude.

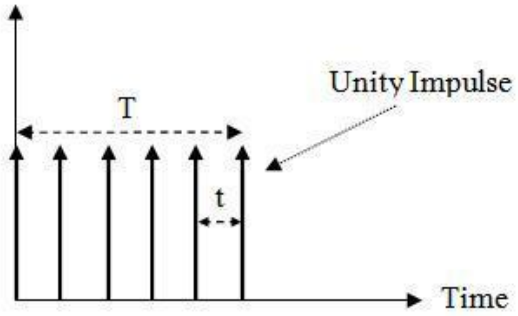

Figure 4-5: Repeated impulse pattern generated while drilling and its characteristics

For a specific drill bit, these two parameters can be calculated as:

$$T = \frac{60}{Bit\ Speed\ (rpm)} \times \frac{d}{D} \tag{4-1}$$

$$t_{spacing} = \frac{T}{N} \tag{4-2}$$

Where *D* is the bit's diameter, *d* is the diameter of the row which locates at the outer diameter of the drill bit, and *N* is number of inserts on the desired row. It should be noted that the second parameter (t) is due to the fact that the inserts are distributed evenly around the cone. The amounts of these parameters

depend on the rotational speed of the cone, which is proportionally related to the bit's speed. This specific pattern is repeated constantly while the cone rotates. Figure 4-6 illustrates these dimensions for a sample cone.

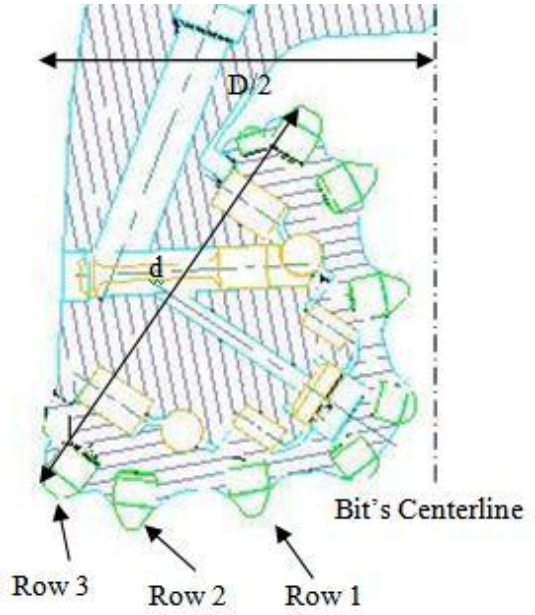

Figure 4-6: A sample rotary cone and related dimensions (ROTACAN)

Chapter 5
Insert Pattern Optimization Procedure

5.1 Outline

In this chapter, the objective function and design parameters for the optimization process are presented. The geometrical constraint that must be applied to the optimization process is also discussed. The Genetic Algorithm has been presented as the optimization method. The system characteristics used for further simulations are also specified.

5.2 General Idea Statement

As described in Chapter 4 in the excitation model, the timings between impulses depend on the configuration of the inserts on the desired row of a cone. If the inserts are distributed evenly, an identical spacing time is used for all following inserts; however, if the inserts are not distributed evenly, a new type of input will be induced. In this case, the time between the impulses will differ as the cone rotates; more specifically, the set of applied impulses will now have an irregular pattern. Figure 5-1 illustrates an example of these two different patterns on a 6-inserts row.

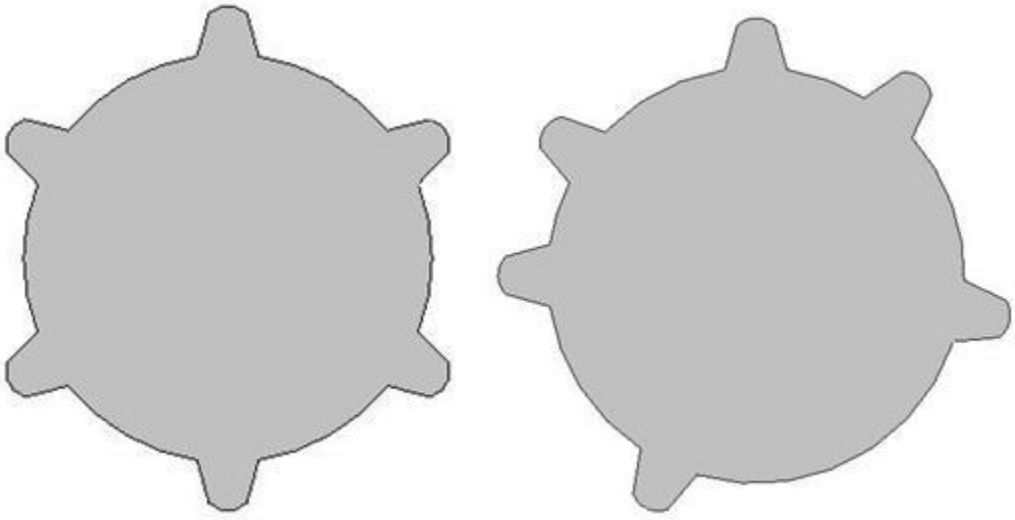

Figure 5-1: Even and irregular distribution of inserts on a cone's row

In Figure 5-2 the blue, curve shows the response of a mechanical system to an impulsive input. As shown in the figure, the response includes both positive and negative amplitudes. The red curve shows the response of the system to a secondary impulse happening with a delay.

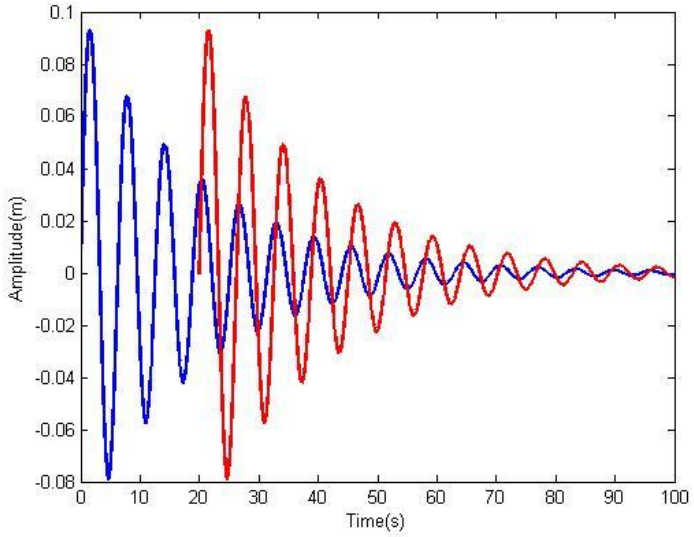

Figure 5-2: Responses for impulsive inputs with delay

The timings between the impulses of the described input can be tuned to reduce the overall system's vibrations. As mentioned previously, tuning the timings of impulses is the core idea of the input shaping method used to suppress residual vibrations in flexible systems. Moreover, the variable pitch cutters used for milling showed the effectiveness of irregular pattern inputs for reducing chatter vibrations. While the impulses in the proposed model have identical amplitudes, the timings between the sequential impulses can be tuned to reduce vibrations of the system. Using the genetic algorithm method, the optimum pattern of impulses in the excitation model can be determined in order to reduce the vibrations of the drillstring.

5.3 Objective Function and Design Parameters

A drillstring is the part of a drilling assembly that transfers rotary motion to a well downhole while drilling. Some of the total energy transferred by the drillstring is absorbed by itself, as kinetic and potential energies. Part of this total absorbed energy is induced by drillstring vibrations. In other words, the drillstring vibrations consume some of the total energy provided by uphole machines; therefore a reduction in drillstring vibrations would allow more energy to be used for drilling action, resulting in more efficient drilling performance.

As mentioned previously, various sources may cause different modes of vibrations in a drillstring. Drill bit-formation interaction is identified as the main cause of vibrations when drilling with rotary cone bits. It is generally understood that part of the vibration excitation phenomenon is related to the design of the drill bit.

The objective function in this investigation is the total energy of drillstring vibrations induced by bit-formation interaction. By reducing this energy, the overall vibrations of the drillstring can be suppressed, resulting in higher performance of drilling. To measure this objective function, the "root mean square" (RMS) of the total energy is calculated for the duration of one revolution of the cone, specified beforehand as T; this interaction is modeled as a set of repeated impulses, therefore, the current design of rotary cones results in a type of input that has an evenly distributed pattern. In this study, the timings between the repeated impulses are used as design parameters of the optimization process to minimize the prescribed objective function. These timings represent the angular spaces between the inserts on a specific row.

5.4 Geometrical Constraint

The geometry of inserts restricts the number of inserts on a specific row of a cone. The angular space between two sequential inserts is shown in Figure 5-3 as θ. For a typical medium-size rotary drill bit, the minimum of this angle is 9 *degrees*. Eventually, a constraint should be applied to the optimization process to satisfy this condition.

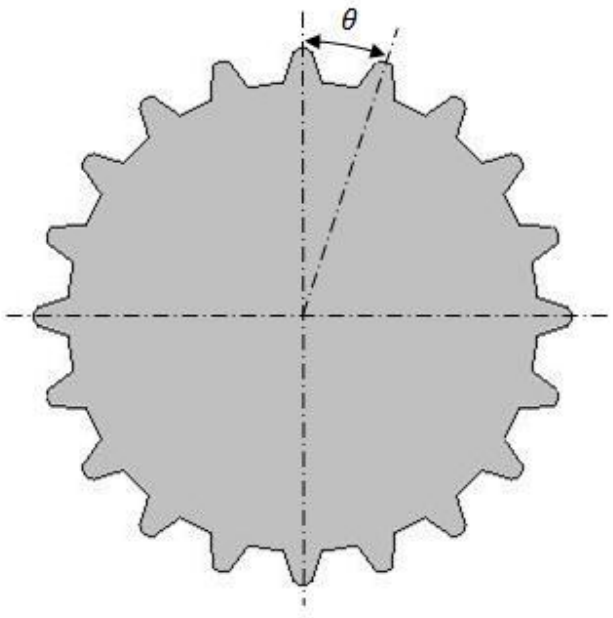

Figure 5-3: Configuration of inserts around the row of the cone for 20 inserts

5.5 System Characteristics

The response of the proposed system, which is used to calculate this total energy, consists of the overall response to the specific excitation defined in previous chapter. The characteristics of such input are identified by the rotary speed of the bit, the number of inserts on a specific row, and the spaces between inserts identifying the timings between induced impulses. While these timings are used as the design parameters in the optimization process, the other two characteristics must be identified to introduce the final input to the system. Therefore, three rotary speeds of the drill bit are considered including 60, 90, and 150 *rpm*, as well as two numbers of inserts, including 6 and 20 inserts. The ratio of d/D, which shows the diameter of the cone per the bit's diameter, is also considered to be equal to 2 for a medium-size rotary cone bit. A 1% structural damping ratio is considered for further analyses.

Finally, it is important to calculate the RMS of the function for the steady-state response of the system; this ensures that any change in the amount of RMS correlates with the changes made in the design parameters. The system's response to a set of repeated impulses over one revolution of the cone for all three modes of vibrations, all three rotary speeds, and two different numbers of inserts are shown in Figures 5-4 to 5-9. The steady state of responses can be easily identified through these plots.

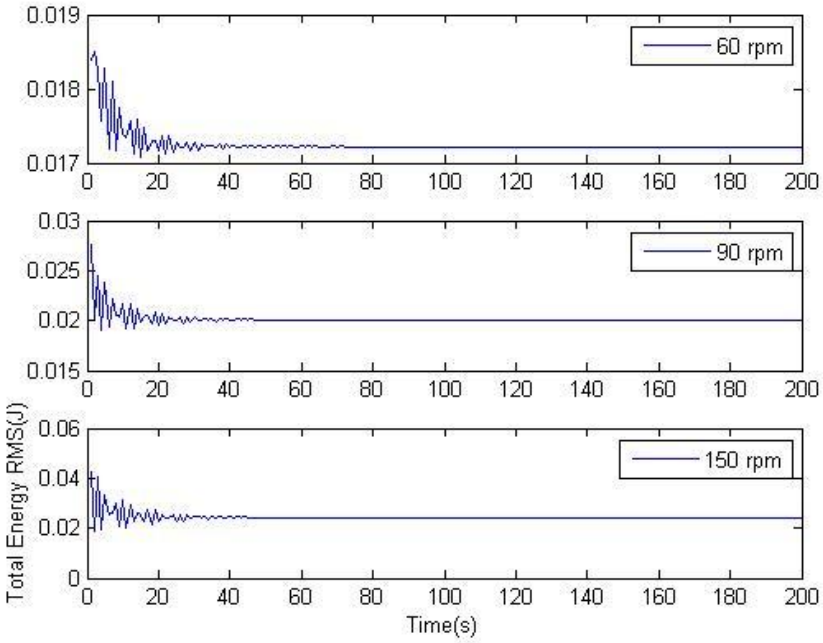

Figure 5-4: RMS of the total energy of lateral vibrations versus time for a 6-inserts row

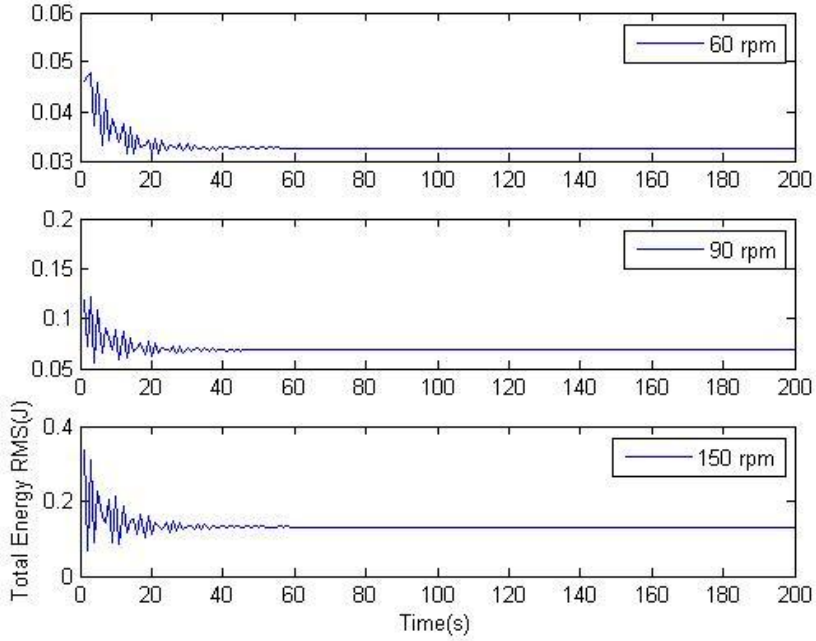

Figure 5-5: RMS of the total energy of lateral vibrations versus time for a 20-inserts row

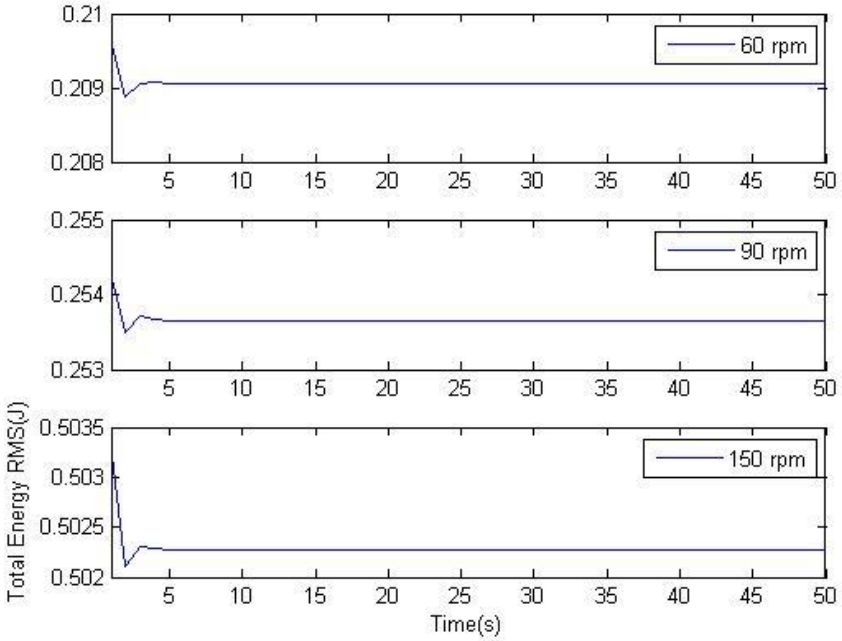

Figure 5-6: RMS of the total energy of torsional vibrations versus time for a 6-inserts row

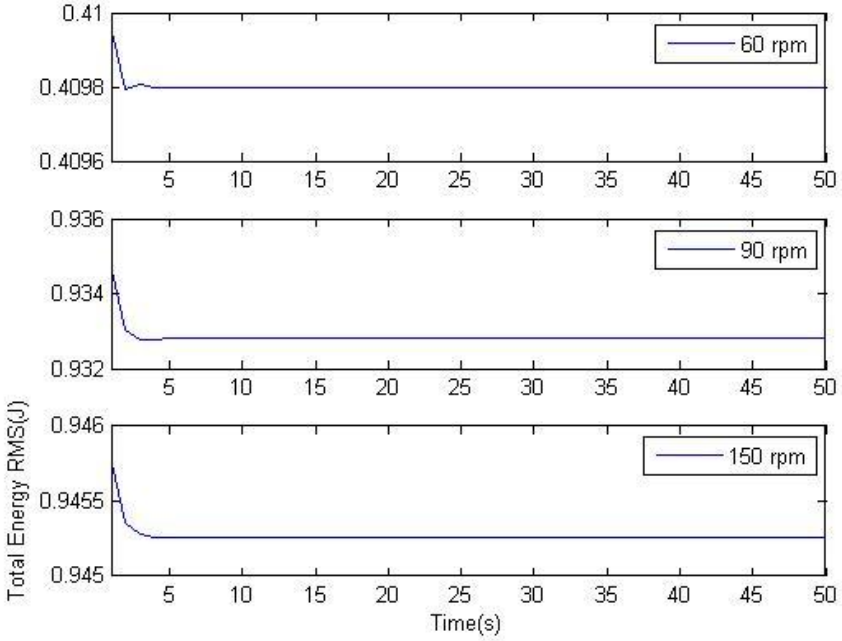

Figure 5-7: RMS of the total energy of torsional vibrations versus time for a 20-inserts row

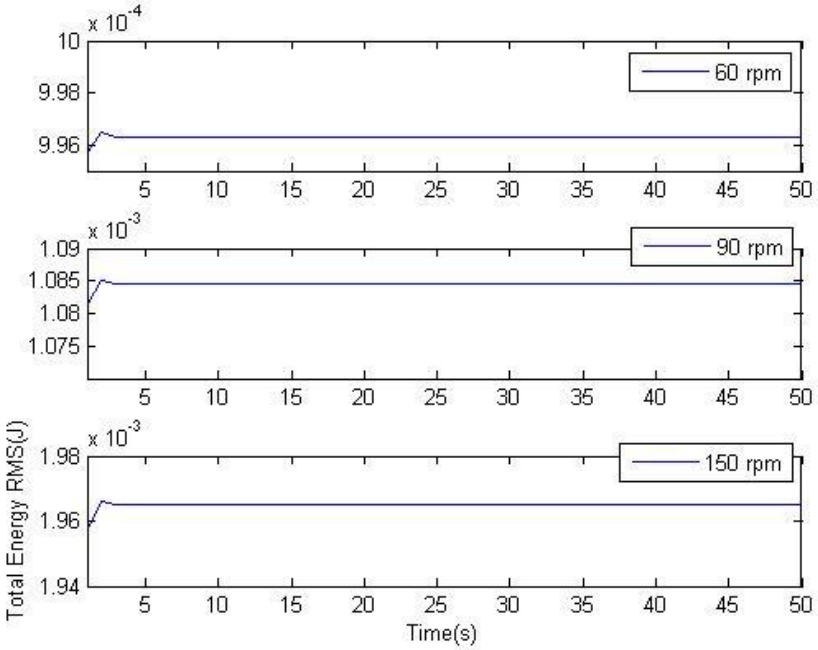

Figure 5-8: RMS of the total energy of axial vibrations versus time for a 6-inserts row

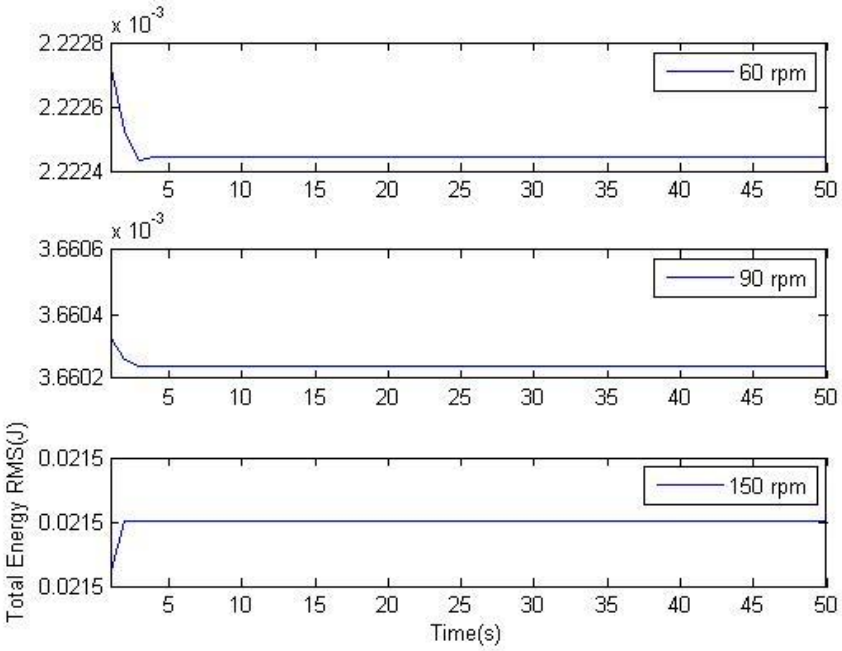

Figure 5-9: RMS of the total energy of axial vibrations versus time for a 20-inserts row

5.6 Optimization Method

Selecting an appropriate optimization method is important due to the large numbers of parameters that must be tuned simultaneously during the optimization process. The required processing time and the required computer memory are also important considerations for large problems such as this.

The genetic algorithm method is one the most powerful methods for solving such problems. This method acts in a comprehensive and simultaneous manner toward finding the global optimum, and due to its nature, reduces the chance of finding a local optimum. The genetic algorithm method can also easily handle problems with large population of parameters. Therefore, it was determined that this method was the most appropriate method for the optimization process.

The "Genetic Algorithm Toolbox" of MATLAB was used for the optimization process. The default settings of the algorithm's parameters have been used to run the simulations, as specified in Table 5-1**Error! Reference source not found.**:

Table 5-1: Genetic Algorithm Method Specifications

Specifications	Description
Population type	Double vector
Population size	20
Fitness scaling	Rank
Selection	Stochastic uniform
Mutation function	Gaussian
Mutation scale	1
Mutation shrink	1
Cross over	Scattered
Stall time Limit	10000 s

Chapter 6
Insert Pattern Optimization Results

6.1 Outline

The results of the optimization process are discussed in this chapter. Optimum configurations of inserts for different number of inserts, different rotary speeds, and different modes of drillstring vibrations are presented.

6.2 Optimum Configurations of Inserts for Each Rotary Speed

6.2.1 Lateral Vibrations

A modal analysis is conducted on the proposed model to obtain the natural frequencies of lateral vibrations. To validate the results, they have been compared to the natural frequencies predicted by Chevallier's model which shows a very close tie between the models. Table 6-1 shows the first nine frequencies.

Table 6-1: Natural frequencies for lateral vibrations

Modes	1	2	3	4	5	6	7	8	9
Chevallier's Model (Hz)	1.54	2.56	3.99	7.85	10.62	16.02	17.77	22.95	27.77
New Model (Hz)	1.44	2.70	3.98	8.27	10.62	15.54	17.63	22.89	29.68

The genetic algorithm has been applied to determine the optimum configuration of inserts for different rotary speeds and different numbers of inserts. Table 6-2 shows the original and optimum configurations for three rotary speeds for a 6-inserts-row. It also shows the percentage of reduction in total absorbed energy realized with each configuration. The final three rows of each table show the percentage of increase or decrease in total absorbed energy if the pattern shown at the same column is applied for the other rotary speeds:

Table 6-2: Optimum patterns for the 6-inserts row (lateral vibrations)

Rotary Speed (rpm)	Original	60	90	150
Configuration of inserts (Degree)	0	0	0	0
	60	57	66	62
	120	121	103	121
	180	185	207	179
	240	248	240	286
	300	306	323	337
Total Energy RMS Reduction %	**-**	***58***	***48***	***13***
Change in Total Absorbed Energy (%)	60 rpm	-	+10	+78
	90 rpm	-10	-	+14
	150 rpm	-15	+69	-

As shown in the table, irregular distribution of inserts can result in a considerable reduction in absorbed energy compared to even distribution. For example, the optimum pattern found for 60 *rpm* rotary speed of the drillstring results in 58% reduction in the total absorbed energy in that speed as well as 10% and 15% reductions for 90 *rpm* and 150 *rpm*, respectively. The optimum pattern found for 90 *rpm* rotary speed can reduce the total energy by 48%; however, applying this pattern for 60 *rpm* and 150 *rpm* results in 10% and 69% increase in total absorbed energy, respectively.

Figure 6-1 shows the total energy RMS versus time for all three rotary speeds including the original and optimum plots.

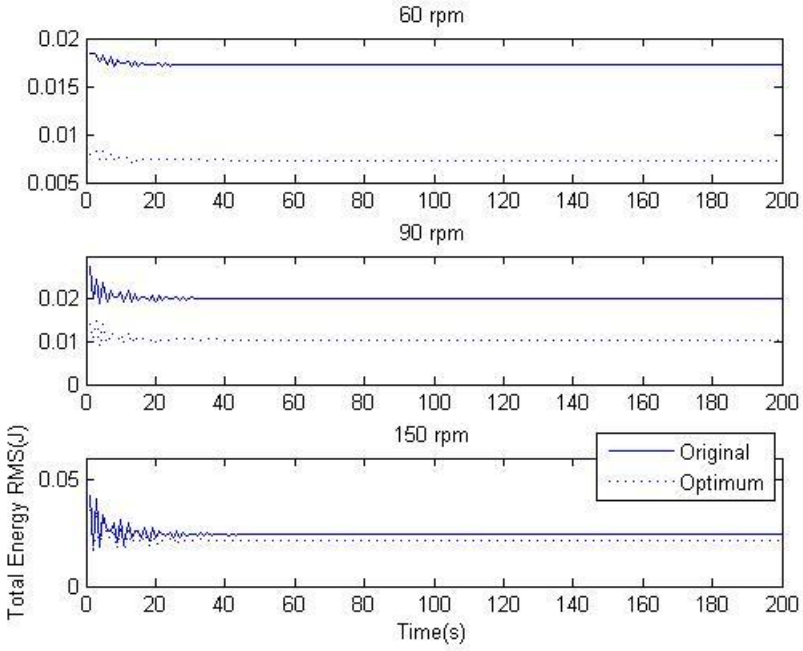

Figure 6-1: Total energy RMS vs. time for different rotary speeds for the 6-inserts row (lateral vibrations)

Table 6-3 shows the original and optimum configurations for a 20 inserts-row.

Table 6-3: Optimum patterns for the 20-inserts row (lateral vibrations)

Rotary Speed (rpm)	Original	60	90	150
Configuration of inserts (Degree)	0	0	0	0.00
	18	17	20	18.00
	36	36	35	36.00
	54	55	58	54.00
	72	70	72	72.00
	90	89	95	90.00
	108	107	110	108.00
	132	127	130	131.63
	146	144	143	146.24
	162	160	168	162.00
	183	179	180	183.12
	201	198	203	200.81
	216	214	215	216.00
	234	233	239	234.00
	252	253	252	252.00
	272	271	275	271.93
	290	289	288	290.00
	309	305	311	308.57
	327	324	324	326.93
	342	343	346	342.00
Total Energy RMS Reduction %	**-**	***16***	***22***	***6***
Change in Total Absorbed Energy (%)	60 rpm	-	-2	+6
	90 rpm	+6	-	+1
	150 rpm	+7	-7	-

As can be seen in the Table 6-3, optimum irregular patterns found for the 60 *rpm* and 90 *rpm* rotary speeds reduce the RMS of the system's total energy, but for 150 *rpm* the optimum pattern is not significantly different from the original one, therefore less improvement is observed. This fact can be understood in the way that while the number of inserts are increased and the overall rotation time is reduced, the timings between sequential impulses cannot be tuned effectively, resulting in less reduction in RMS value. Figure 6-2 shows a comparison of the RMS versus time plot for the original and optimum patterns for each rotary speed.

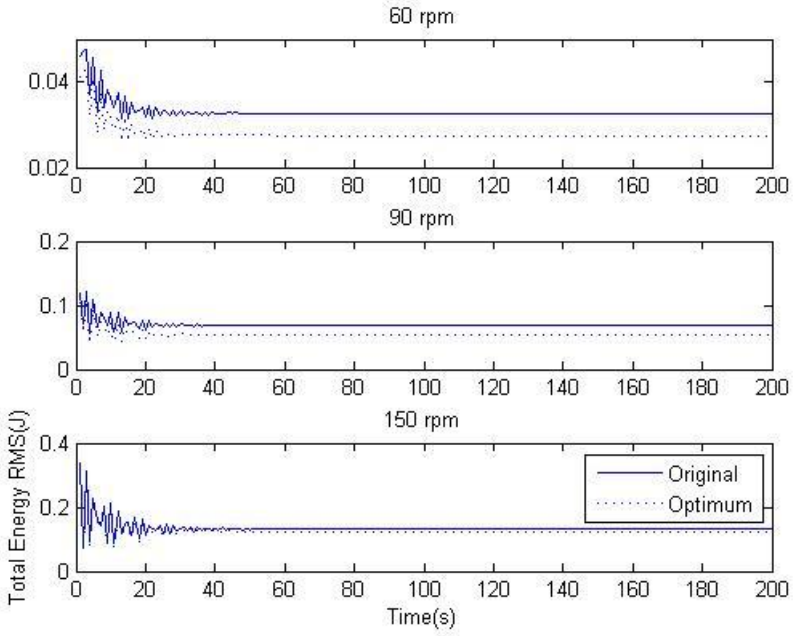

Figure 6-2: Total energy RMS vs. time for different rotary speeds for the 20-inserts row (lateral vibrations)

6.2.2 Torsional Vibrations

Table 6-4 shows the natural frequencies for the five first modes.

Table 6-4: Natural Frequencies for torsional vibrations

Modes	1	2	3	4	5
Natural Frequencies (Hz)	20.7	62.4	104.6	147.9	192.5

To validate these results, the first torsional natural frequency for a beam element can be calculated analytically. For a beam with the clamped-free boundary condition, the first natural frequency is expressed as:

$$\omega_n = \left(\frac{k_e}{m_e}\right)^{0.5} = \left(\frac{G/l}{\rho l/3}\right)^{0.5} = \left(\frac{3G}{\rho}\right)^{0.5}\left(\frac{1}{l}\right) \quad (6\text{-}1)$$

Considering $G = 79.3\ GPa$ and $\rho = 7833\ kg.m^{-3}$, the natural frequency of such an element can be expressed in terms of *Hertz* as:

$$\omega_n = \frac{877}{l} \quad (6\text{-}2)$$

Therefore, for the new model with a length of 38.4 m, the first torsional natural frequency is equal to 22.8 *Hz*, which is very close to the results predicted by the model.

Table 6-5 shows the original and optimum configurations for three rotary speeds for a row with 6 inserts. It also shows the percentage of reduction in total absorbed energy realized with each configuration. The last three rows show the percentage of increase or decrease in the total absorbed energy if the pattern shown in the same column is applied for other rotary speeds.

Table 6-5: The optimum configurations for the 6-inserts row (torsional vibrations)

Rotary Speed (rpm)	Original	60	90	150
Configuration of inserts (Degree)	0	0	0	0
	60	50	61	79
	120	101	120	130
	180	132	181	205
	240	148	240	245
	300	268	301	313
Total Energy RMS Reduction %	**-**	***16***	***12***	***40***
Change in Total Absorbed Energy (%)	60 rpm	-	-11	+22
	90 rpm	+176	-	+31
	150 rpm	+21	0	-

As shown in the table, irregular distribution of inserts can result in a considerable reduction in absorbed energy compared to the original, regular distribution. Figure 6-3 shows the total energy RMS versus time for all three rotary speeds, including the original and optimum plots.

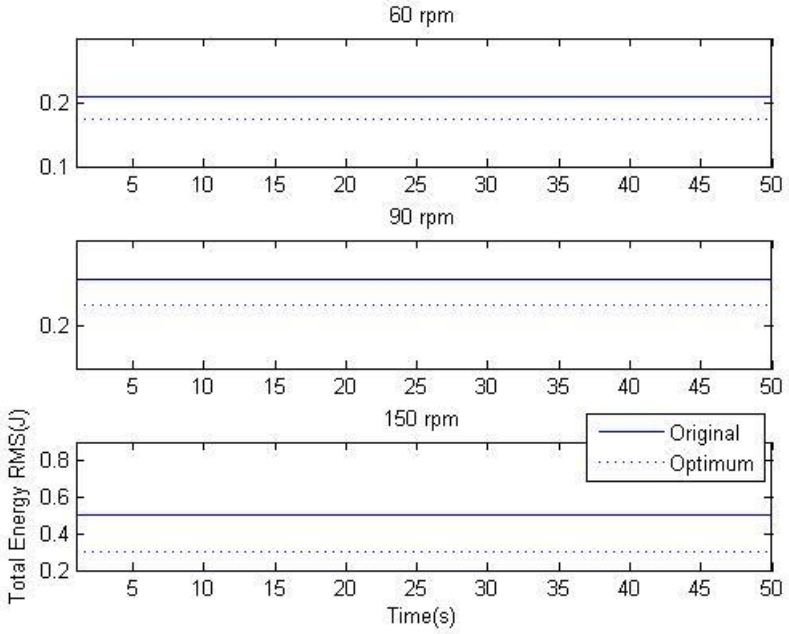

Figure 6-3: Total energy RMS vs. time for different rotary speeds for the 6-inserts row (torsional vibrations)

Table 6-6 shows the original and optimum configurations for a row with 20 inserts.

Table 6-6: The optimum configurations for the 20-inserts row (torsional vibrations)

Rotary Speed (rpm)	Original	60	90	150
Configuration of inserts (Degree)	0	0	0	0
	18	18	25	18
	36	36	36	36
	54	54	51	54
	72	72	73	72
	90	90	92	90
	108	108	105	108
	132	125	128	126
	146	144	149	144
	162	162	162	161
	183	180	180	180
	201	198	205	198
	216	216	227	215
	234	234	239	234
	252	252	252	252
	272	270	270	270
	290	288	298	288
	309	306	317	306
	327	325	326	324
	342	342	336	342
Total Energy RMS Reduction %	**-**	***1***	***44***	***2***
Change in Total Absorbed Energy (%)	60 rpm	-	+185	+5
	90 rpm	+2	-	+1
	150 rpm	+4	+39	-

As can be seen in Table 6-6, the optimum patterns found for 60 and 150 *rpm* rotary speeds are slightly different from the original patterns, consequently there is no considerable reduction in RMS values, although the optimum configuration found for 90 *rpm* can effectively reduce the RMS value. Figure 6-4 shows a comparison of the RMS versus time plot for the original and optimum patterns for each rotary speed.

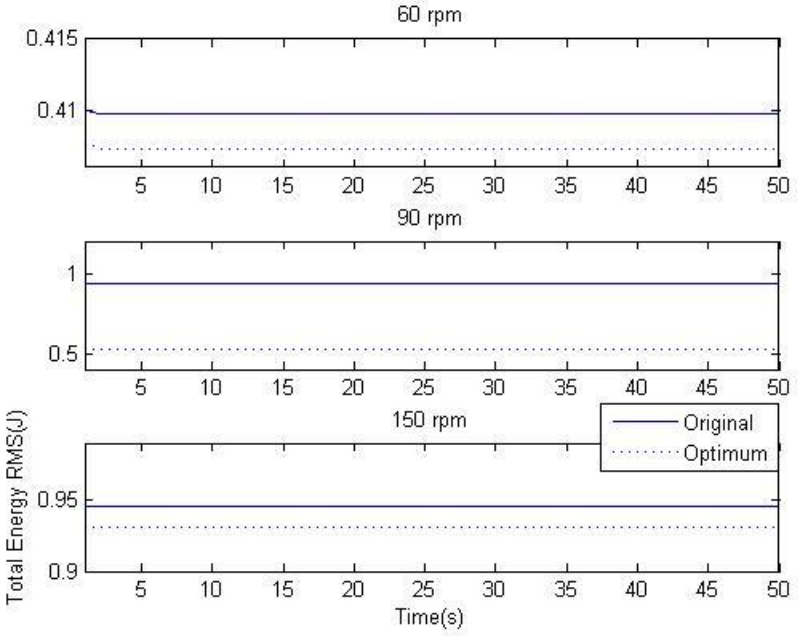

Figure 6-4: Total energy RMS vs. time for different rotary speeds for the 20-inserts row (torsional vibrations)

6.2.3 Axial Vibrations

Table 6-7 shows the natural frequencies for the five first modes.

Table 6-7: Natural frequencies for axial vibrations

Modes	1	2	3	4	5
Natural Frequencies (Hz)	33.5	100.8	169.0	238.9	311.1

To validate these results, the first axial natural frequency for a beam element can be calculated analytically. For a beam with the clamped-free boundary conditions, the first natural frequency is expressed as:

$$\omega_n = \left(\frac{k_e}{m_e}\right)^{0.5} = \left(\frac{EA/l}{\rho Al/3}\right)^{0.5} = \left(\frac{3E}{\rho}\right)^{0.5}\left(\frac{1}{l}\right) \quad (6\text{-}3)$$

Considering $E = 207\ GPa$ and$\rho = 7833\ kg.m^{-3}$, the natural frequency of such an element can be expressed in term of Hz as:

$$\omega_n = \frac{1417}{l} \quad (6\text{-}4)$$

Therefore, for the new model with a length of 38.4 *m*, the first axial natural frequency is equal to 36.9 *Hz*, which is again very close to the results predicted by the model.

Table 6-8 shows the original and optimum configurations for three rotary speeds for a row with 6 inserts. It also shows the percentage of reduction in total absorbed energy realized with each configuration. The final three rows also show the percentage increase or decrease in total absorbed energy if the pattern shown in the same column is applied for other rotary speeds:

Table 6-8: The optimum configurations for the 6-inserts row (axial vibrations)

Rotary Speed (rpm)	original	60	90	150
Configuration of the inserts(degree)	0	0	0	0
	60	61	14	14
	120	118	120	86
	180	180	135	169
	240	263	240	274
	300	342	255	299
Total Energy RMS Reduction %	**-**	***10***	***4***	***23***
Change in Total Absorbed Energy (%)	60 rpm	-	+11	+8
	90 rpm	0	-	-9
	150 rpm	-17	-25	-

As can be seen in Table 6-8, the optimum irregular configurations are more effective in reducing the RMS value for 60 and 150 *rpm* rotary speeds than the one found for 90 *rpm*.

Figure 6-5 shows the total energy RMS versus time for all three rotary speeds including the original and optimum plots.

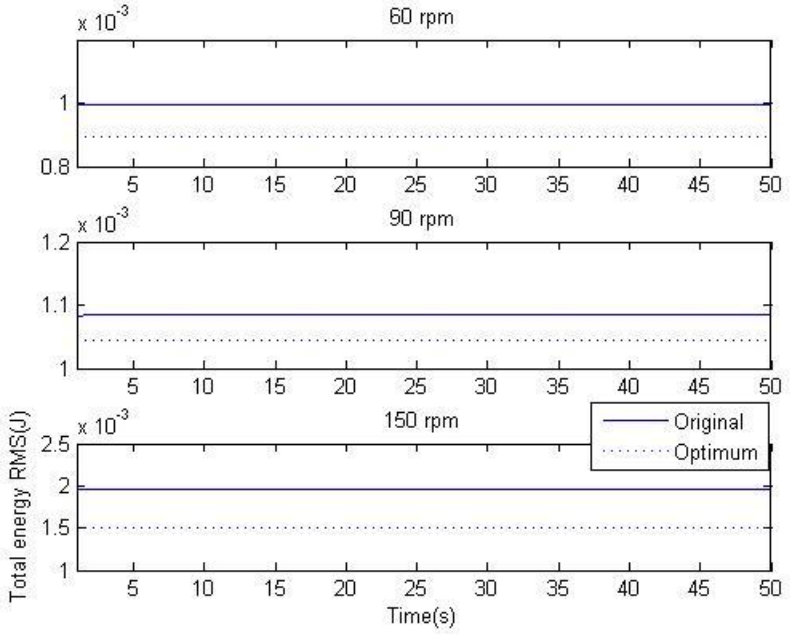

Figure 6-5: Total energy RMS vs. time for different rotary speeds for the 6-inserts row (axial vibrations)

Table 6-4 shows the original and optimum configurations for a row with 20 inserts. The irregular patterns reduced the total absorbed energy by an acceptable amount.

Table 6-9: The optimum configurations for the 20-inserts row (axial vibrations)

Rotary Speed (rpm)	Original	60	90	150
Configuration of inserts	0	0	0	0
	18	18	16	26
	36	37	36	41
	54	54	52	58
	72	73	72	75
	90	90	88	90
	108	109	105	107
	132	127	127	118
	146	149	142	136
	162	162	162	162
	183	180	178	173
	201	202	195	189
	216	216	216	214
	234	235	231	229
	252	252	249	245
	272	271	266	261
	290	289	286	289
	309	306	305	310
	327	325	320	324
	342	342	341	338
RMS Reduction %	**-**	***17***	***37***	***84***
Change in Total Absorbed Energy (%)	60 rpm	-	+9	+43
	90 rpm	+10	-	+32
	150 rpm	-6	+5	-

Figure 6-6 shows a comparison of the RMS versus time plot for the original and optimum patterns for each rotary speed.

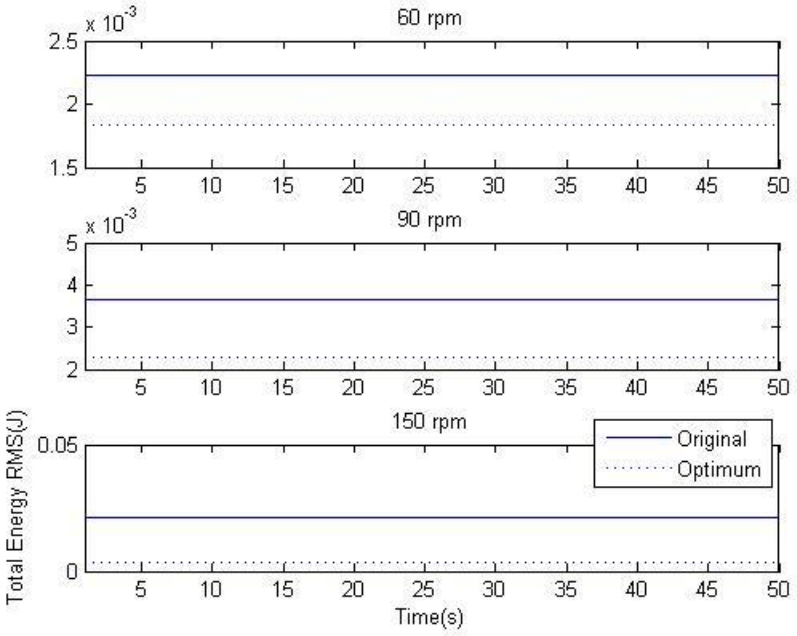

Figure 6-6: Total energy RMS vs. time for different rotary speeds for the 20-inserts row (axial vibrations)

6.3 Optimum Configurations of Inserts for a Range of Operating Rotary Speeds

As discussed in the previous section, the optimum distribution of inserts can be found for specific rotary speeds. According to the results, each speed possesses its unique configuration, which, if applied to the other rotary speeds, may decrease or increase the total energy of the system. These results are helpful in cases where the bits are working at a specific operating speed; however, in some cases, a bit may work with different speeds during one operation. For such cases, the optimum configuration should be found to minimize the total energy of the drillstring during the entire operation.

In this section, three rotary speeds equal to 60, 75, and 90 *rpm* are considered as the range of speeds for a rotary cone bit. Using the average of the total energy for those speeds, it is possible to find the configurations of inserts that minimize the total energy for the whole range of speeds. Table 6-10 and Table 6-11 present the optimum distributions for the 6-inserts and 20-inserts rows for different modes of vibrations. As can be seen in the tables, the optimum configurations of inserts can reduce the RMS values for different modes of vibrations and different number of inserts, except for the pattern found for the torsional vibrations of the 6-inserts row. In the latter case, the optimum pattern is slightly different from the original one and low reduction in the RMS value result is expected.

Table 6-10: Optimum Configurations for the 6-inserts row

Rotary Speed (rpm)	Original	Lateral	Torsional	Axial
Configuration of the inserts (degree)	0	0	0	0
	60	26	60.02	71
	120	102	120.00	120
	180	125	180.08	166
	240	203	239.65	240
	300	261	299.59	314
Total Energy RMS Reduction %	**-**	***29***	***1***	***10***
Change in Total Absorbed Energy (%)	60 rpm	-37	-3	-5
	75 rpm	-16	-1	-21
	90 rpm	-29	+1	+11

Table 6-11: Optimum Configurations for the 20-inserts row

Mode	Original	Lateral	Torsional	Axial
Configuration of inserts	0	0	0	0
	18	18	19	18
	36	34	36	35
	54	55	55	50
	72	73	73	66
	90	99	92	88
	108	115	109	102
	132	128	125	124
	146	155	144	142
	162	166	162	162
	183	177	180	180
	201	205	199	200
	216	231	216	216
	234	242	236	237
	252	261	252	249
	272	272	269	270
	290	288	290	285
	309	318	306	305
	327	330	327	323
	342	348	342	338
Total Energy RMS Reduction %	**-**	***51***	***28***	***16***
Change in Total Absorbed Energy (%)	60 rpm	+16	+4	+5
	75 rpm	-76	-56	-17
	90 rpm	-17	-7	-27

Chapter 7
Bearing Design Criteria

7.1 Outline

In this chapter, contact stress is presented as the main concept required for bearing design. The extended definition of contact stress has been outlined for roller bearings. The dynamic and static capacities of bearings are reviewed as two main criteria required for designing bearings. The equivalent load calculation and basic dimensions of the tapered roller bearings are presented. The standard formulas for all these aspects are addressed.

7.2 Introduction

Even under the best operating conditions, no bearing has an unlimited lifespan. After a certain time, bearings will not function as effectively or will fail, resulting in a lower efficiency of the device. Surface fatigue has been known to be the main cause of bearing failures. Surface fatigue occurs when metallic particles flake off of the raceways or rolling elements. Different theories describing the process that results in surface fatigue are mainly concerned with the initiation of a crack at a certain depth which propagates to the surface causing the surface fatigue (Harris, 2001).

Despite attempts to predict the lifetime of bearings accurately it has not been possible to predict the exact time of the failure of a bearing. Therefore, a combination of theory and experience has been used to present expressions to predict bearing lifetime. These are known as specific standards which are used to design, fabricate, and operate various types of bearings. These expressions differ according to the type of bearing, the size, and the intended application.

Tapered roller bearings are widely used in industry for various applications, ranging from passenger cars to aerospace vehicles. The unique design of these bearings allows them to withstand both radial and axial forces and reduce the number of elements required for such an application. In this type of bearings, rollers have a conical shape and are located around the raceways such that their axes meet at a single point. Different load capacities are achieved by changing the dimensions of the rollers and raceways and by adjusting the direction of the rollers.

In the next section, the basic dimensions of tapered bearings and the formulas and standards required to design them are presented.

7.3 Contact Stress

7.3.1 Contact Stress Definition

Contact surface stress is defined as stress generated at the contact area of two different surfaces compressing against each other. This contact area can theoretically be defined as a point or a line under a zero load. A point contact can be described for the interaction of a ball and a flat surface, but the line contact represents the contact between a cylinder and a flat surface. For a line contact, the induced contact stress can be calculated using the dimensions in Figure 7-1, as written below (Harris 2001):

$$\sigma_r = \frac{2F\cos\theta}{\pi r} \tag{8-1}$$

Figure 7-1 shows a schematic for the line contact between a cylinder and a surface.

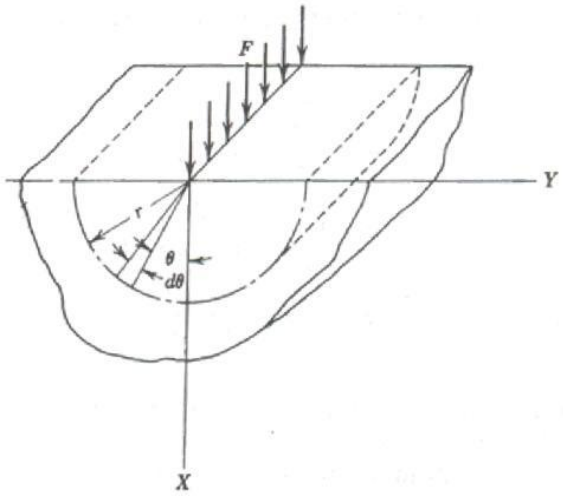

Figure 7-1: Contact stress definition (Harris, 2001)

Under a load, contact areas will grow; eventually a point contact alters to an elliptical shape in the contact zone, while a line contact will form a rectangle on the contact area. Such a phenomenon results in changes in the amount and the distribution of the contact stress. For example, for a line contact the maximum stress induced can be expressed as follows (Harris, 2001):

$$\sigma_{max} = \frac{2Q}{\pi bl} \tag{8-2}$$

Where Q is the applied load and b and l are the width and height of the rectangle, respectively.

Contact stress forms the basis for rolling bearing analyses. This definition can be used to pursue the expressions required to predict the lifetime of bearings, as reviewed in the following.

7.3.2 Contact Stress in Roller Bearings

The contact stress definition can be used to determine the stresses generated on the raceways and roller element surfaces while a bearing operates. The formula for a line contact can be used in this case; however, while the contact area contains more than one surface, it is important to find the distribution of the load over the bearing surfaces. Eventually, the maximum load can be selected as the operating load and crucial areas can be defined. Roller bearings can then be designed taking into account information about load distribution and crucial contact areas.

The maximum force one rolling element can withstand must be determined. There have been numerous attempts to define such a load for various loading conditions. An expression used for radial loads is (Harris, 2001):

$$Q_{max} = \frac{5F_r}{Z \cos \alpha} \tag{8-3}$$

where F_r is the radial load applied to the bearing, Z is the number of rolling elements, and α is the mounted contact angle. A similar expression can be defined for axial loadings as well. For axial loading, it is considered that the axial load is distributed evenly among the rollers (Harris, 2001):

$$Q = \frac{F_a}{Z \sin \alpha} \tag{8-4}$$

In this expression F_a represents the axial load on the bearing.

7.4 Bearing Life Prediction

7.4.1 General Expression

As discussed previously, there have been various attempts to relate the life of bearings to the applied load and the specifications of the bearings. Generally, this relation can be defined as follows:

$$\frac{L_1}{L_2} = \left(\frac{Q_2}{Q_1}\right)^n \tag{8-5}$$

where L shows the lifetime, Q represents the load value, and n depends on the type of the bearings, which is 3 for ball bearings and $3\frac{1}{3}$ for cylindrical rollers.

Moreover, the life of bearings for a specific load can be related to its life for another load. The value of this time depends on the probability of survival for bearings. For example, one can define a lifetime in which 90% of bearings endure a specific load. Therefore, for a specific load and a specific probability of survival, a predicted lifetime can be calculated.

7.4.2 Dynamic Capacity

Based on the aforementioned formula for predicting the life of bearings, the basic dynamic capacity of a rolling bearing can be defined in terms of the load that can be endured by the bearings for a specific probability of survival of bearings for one million revolutions. Therefore, by determining the dynamic capacity of a bearing, the bearing life can be calculated in terms of a million revolutions for a specific probability of survival, usually 90%.

Different formulas have been proposed for the dynamic capacity calculation, but the most widely-used are those which are prescribed by international organizations, such as ISO and ANSI, and are known as bearing standards. To calculate the dynamic capacity of roller bearings, the formula presented by ANSI (Standard 11-1990) is shown below:

$$C = f_{cm}(il\cos\alpha)^{7/9}Z^{3/4}D^{29/27} \tag{8-6}$$

where f_{cm} is a factor defined by specific tables proposed in the aforementioned standard, i is the number of rows, l is the effective roller length, α is the contact angle, Z is the number of roller elements, and D is the roller diameter. The selection of the f_{cm} values from the standard tables is based on another value defined as (Harris, 2001):

$$\gamma = \frac{D\cos\alpha}{d} \tag{8-7}$$

where d is the mean diameter of the bearing, defined as the average of the inner and outer raceways' diameters.

7.5 Static Capacity

Static capacity is used to identify the allowable amount of deformation in bearings' races. Exceeding the allowable deformation may cause excessive vibrations and stress concentrations, which can affect the operation of bearings. A definition used by Harris states: "the static capacity of the bearings is the load applied to non-rotating bearings which results in a permanent deformation equal to *0.0001 D* at the weaker of the inner or outer raceway contacts occurring at the position of the maximum loaded rolling element",(2001).

Different expressions have been proposed to define this capacity as well. In this study the formula presented by ISO (ISO 76:1989) is used:

$$C_s = 44(1-\gamma)ilZD\cos\alpha \tag{8-8}$$

7.6 Equivalent Loads

The final step in the calculation of bearing life and static capacity of bearings is definition of the load required for the aforementioned formulas. The importance of this definition becomes clear due to the combination of axial and radial forces that are applied to the bearings. The formulas presented by Harris to calculate the equivalent value for dynamic and static loads. For dynamic loads the following expression has been used (ANSI Standard 11-1990):

$$F_e = XF_r + YF_a \tag{8-9}$$

where F_r and F_a are the radial and axial forces, respectively. The values of X and Y are defined according to Table 7-1:

Table 7-1: Equivalent contact load for single row roller bearings (ANSI Standard 11-1990)

$F_a/F_r \leq 1.5 \tan\alpha$		$F_a/F_r > 1.5 \tan\alpha$	
X	Y	X	Y
1	0	0.4	$0.4 \cot\alpha$

The same formula can be used to determine the static equivalent load with the coefficients X and Y defined as shown in Table 7-2:

Table 7-2 : Static equivalent load (ANSI Standard 11-1990)

Equivalent Force	Conditions
$F_s = XF_r + YF_a$	$X = 0.5, Y = 0.22 \cot\alpha$
$F_r = F_s$	$F_r < F_s$

7.7 Basic Dimensions of Tapered Roller Bearing

The basic dimensions for a tapered roller bearing have been defined in Figure 7-2. These dimensions can be used for the presented formulas to design a new tapered bearing, as shown in Table 7-3:

Table 7-3: Basic dimensions of tapered roller bearings (Harris, 2001)

Dimensions	Definitions
Mean diameter of the bearing	$d_{mean} = {}^{1}/_{2}\,(d_{bore} + Outer\ Diameter)$
Half of the cone angle	α_i
Half of the cup angle	α_o
Half of the cone backface rib	α_f
Length of the roller element	l_t
Roller angle	α_R
Mean diameter of the roller	$D_m = {}^{1}/_{2}\,(D_{max} + D_{min})$

The coefficient γ can be defined for the inner and the outer raceways of the bearing (Harris 2001) as follows:

$$\gamma_i = \frac{D_m \cos \alpha_i}{d_m} \tag{8-10}$$

$$\gamma_o = \frac{D_m \cos \alpha_o}{d_m} \tag{8-11}$$

Figure 7-2 shows the basic dimensions of a tapered roller bearing.

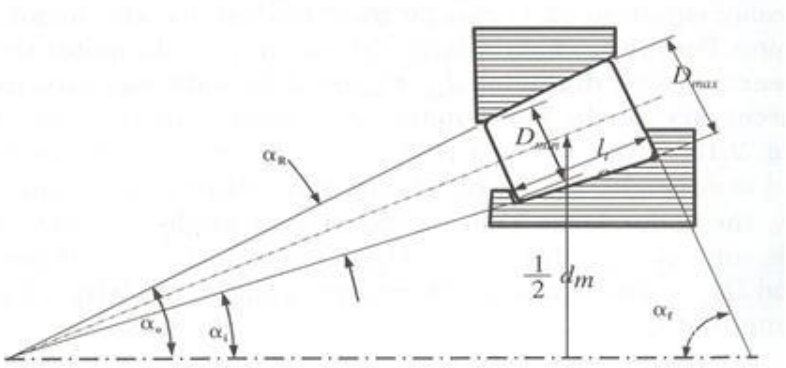

Figure 7-2: Tapered roller bearing (Harris, 2001)

Chapter 8
Rotary Drill Bit Dynamic Analysis and Bearing Design

8.1 Outline

In this chapter, the calculations of forces acting on the bearings are presented. Objective functions have been selected to determine the lifetime and the static capacity of the bearings. The required formulas are provided, design parameters are defined, and final dimensions for the new bearings are calculated.

8.2 Main Objective

As explained in literature review, rotary cone bits face several challenges when used in drilling. These challenges are mainly concerned with bits used for blasthole drilling, as shown in Figure 8-1. As discussed previously, elevated axial forces result in premature failure of the thrust washers used as axial bearings. In addition, cages are not used in the current design, which results in reduced efficiency of the bearings due to the contact between rollers. It is demanded that the bit operates properly for at least 200 hours continuously. Such a demand should be satisfied by the bearings as well.

While blasthole drill bits are cooled by means of air, they are open to the outside environment, which increases the chance of contamination of the bearings. It is therefore necessary to seal off the bearings from exposure to external elements. Such a seal also should be capable of withstanding high pressures and high temperatures upon being employed in harsh environments. Elevated pressures vary from the hundreds of psi for blasthole drilling to thousands of psi for oil drilling, while temperatures may also exceed tens of Fahrenheit. Therefore selecting seals from available commercial products, capable of bearing highest level of pressures and temperatures is demanded. The development of a new method for retaining the cones on the arms as a means of reducing the number of elements used in a bit and simplifying the fabrication process is also an important goal.

In Chapter 8 and Chapter 9, new design for blasthole rotary cone bits which addresses all of the above mentioned problems is introduced. Tapered bearings, which can withstand the generated forces for longer hours, are used instead of the current combination of thrust and roller bearings. A new sealing package has also been designed. The new design also includes the bearing cages and a new retaining method, which can improve the system's performance. The dimensions of the new bearings have been calculated in this chapter and the integrated design is presented in Chapter 9.

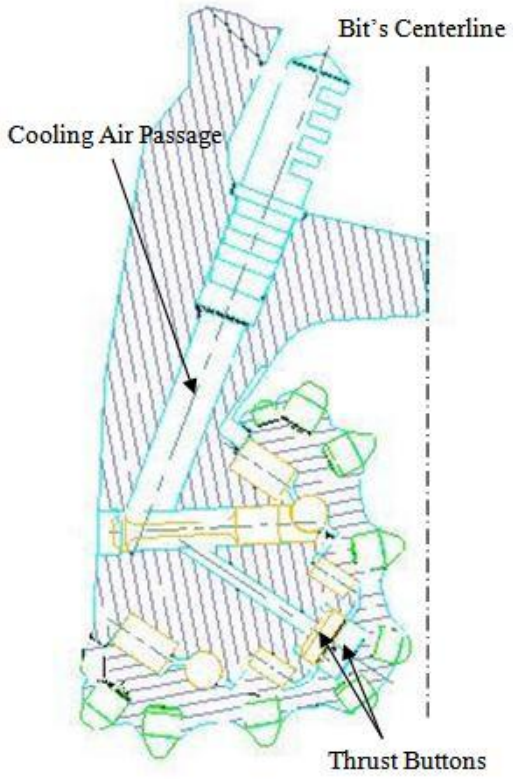

Figure 8-1: Air cooled rotary cone bits for blasthole drilling (ROTACAN)

8.3 Forces

A combination of downward force, known as weight on bit (WOB), and rotary torque act on the rotary drill bit. The downward force provides the force required to crush the rock, while the rotary torque rolls the cones over the rock. Rotary torque, which is generated by the rotary table and transmitted downhole by means of drill pipes, is usually attenuated due to friction with the borehole wall. Therefore it is expected that the actual rotary torque that is produced by the rotary table is not seen downhole; however, as a safety factor, the total rotary torque is considered to be applied to the drill bit. In this section, the total radial and axial forces acting on a cone of the drill bit are calculated and used in the design of the new bearings. A medium-size rotary cone bit, with the specifications shown in Table 8-1 is used as the base for further analyses:

Table 8-1: Specifications of a medium-size rotary cone bit (ROTACAN)

Specification	Value
Model	ROTACAN AP5(#1)
Bit's diameter	$10\,^{5}/_{8}$
WOB per inch of diameter	2000-5000 lbs.
Total WOB per bit	21250-53125 lbs.
Total WOB per each cone	7100-17700 lbs.
Rotary torque	7500-15300 ft-lbs.
Orientation of the cone to the horizon	56^{0}

8.3.1 Radial and Axial Forces Acting on the Bearings

To simplify the analysis, one can consider that the downward force distributed evenly among the bit's diameter, as shown in Figure 8-2. It is assumed there are two bearings inside the cone; therefore, with three cones on a bit, the total downward force can be divided into six equal portions. It should be noted that the maximum value of the WOB is considered for further investigation. The resultant force can also be projected into two axial and radial components with respect to the axis of the cone. Those forces are calculated as:

$$F_{total} = 8850\ lbs \tag{9-1}$$

$$F_{radial} = 7340\ lbs \tag{9-2}$$

$$F_{axial} = 4950\ lbs \tag{9-3}$$

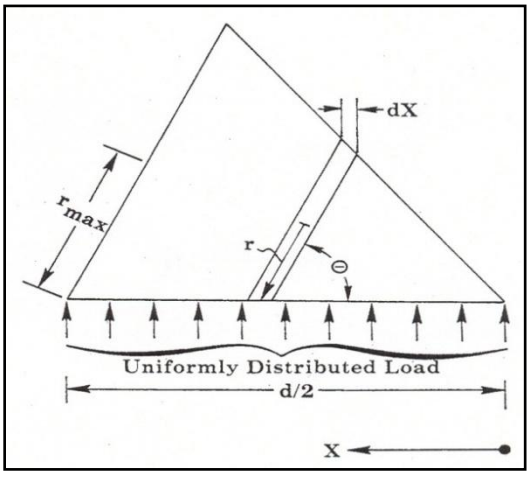

Figure 8-2: Load distribution along the cone (Warren, 1984)

8.3.2 Rotary Torque

The distribution of the forces generated by the rotary cone along the cone's axis must be determined. Assuming that the cone is not twisted while operating, one can also assume that the torque remains constant along the cone's axis. The forces therefore are distributed proportional to distances from the cone's axis and the bit's axis. In Figure 8-3 the outside of the cone has been divided into 6 equal portions. For such the model, one can write:

$$T_1 = T_2 = T_3 = T_4 \quad \Rightarrow \quad F_1 r_1 = F_2 r_2 = F_3 r_3 = F_4 r_4 \tag{9-4}$$

$$\mathrm{T_{total}} = \mathrm{F_1 X_1 + F_2 X_2 + F_3 X_3 + F_4 X_4} \tag{9-5}$$

where *T*, *F*, *r*, and *X* are the torque, force, distance from the cone's axis, and distance from the bit's axis, respectively. It is assumed that one of the bearings is located between points 1 and 2 and the other is located between points 3 and 4. The mean forces acting on those two bearings due to the rotary torque can then be calculated as:

$$F_{1-2} = 7725\ lbs \tag{9-6}$$

$$F_{3-4} = 4575\ lbs \tag{9-7}$$

While these forces are acting radially with respect to the cone's axis, the total radial and axial forces acting on each bearing can be calculated. For the bearing which is located near the cone's mouth (referred to as the back bearing), we have:

$$F_{radial\ -b} = 8650\ lbs \tag{9-8}$$

$$F_{axial\ -b} = 4950\ lbs \tag{9-9}$$

And for the bearing which is located on the front head (known as front bearing) we have:

$$F_{radial\ -f} = 10655\ lbs \tag{9-10}$$

$$F_{axial\ -f} = 4950\ lbs \tag{9-11}$$

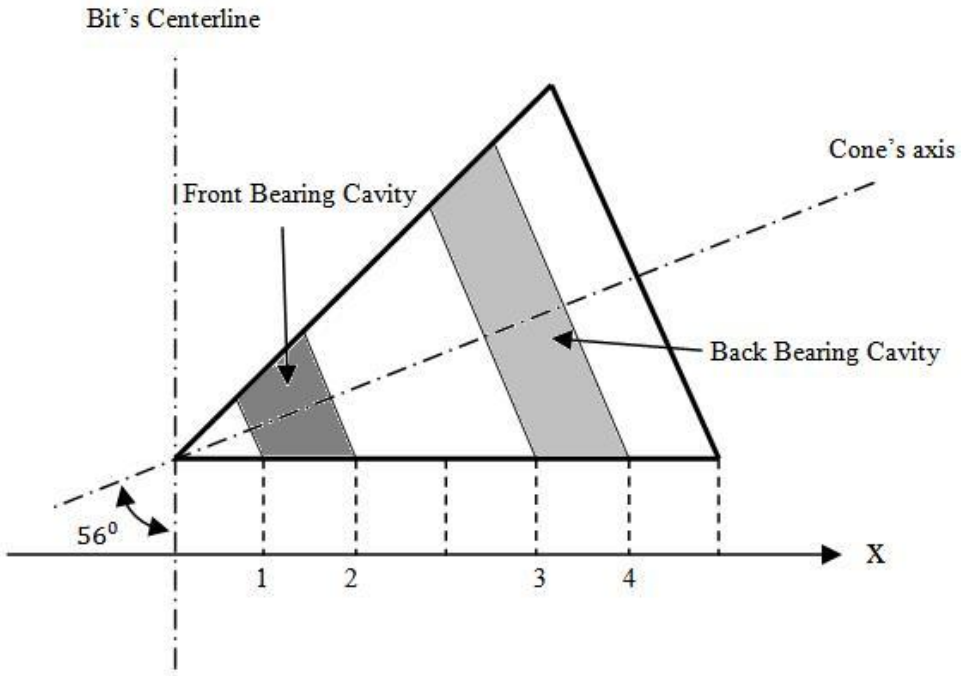

Figure 8-3: The cone

8.4 Objective Functions and Design Parameters

As mentioned previously, two important criteria are considered while designing the bearings. The lifetime and static capacity of the bearings are the criteria which assure the proper operation of the bearings for a desired period of time. The formulas required to design the new bearings are summarized in Table 8-2:

Table 8-2: Formulas for bearing design

Description	formula
Life (million revolutions)	$L = \left(\frac{C}{Q}\right)^{10/3}$
Static capacity (lbs./inch)	$C_s = 44(1-\gamma)ilZD\cos\alpha$
Dynamic Capacity (lbs./inch)	$C = f_{cm}\,(il\cos\alpha)^{7/9} Z^{3/4} D^{29/27}$
Maximum load	$Q_{max} = \frac{5F_r}{Z\cos\alpha}$

Some formulas were derived to relate the bearing's dimensions to the mentioned objective functions, as described in Appendix A. Consequently, it is possible to design the new bearings according to the parameters outlined in Table 8-3:

Table 8-3: Design parameters

Design parameters	Definition
Mean diameter of the bearing	$d_{mean} = {}^{1}/_{2}\,(d_{bore} + Outer\ Diameter)$
Half of the cone angle	α_i
Half of the cup angle	α_o
Length of the roller element	l_t
Minimum diameter of the roller element	D_{min}
Number of rollers	Z

8.5 Results

Through a trial-and-error process, a set of parameters was found that satisfies the requirements for the new bearings. While the inside cavity of the cone is limited due to the presence of the inserts' holes, the dimensions must be checked after each trial to make sure that there is no conflict between the bearing cavity and the holes. The final results for the back and front bearings are summarized in Table 8-4:

Table 8-4: New bearings' dimensions

Parameters	Values	
	Back Bearing	Front Bearing
Mean diameter of the bearing (Inches)	3.0	1.5
Cone angle (Degrees)	23	23
Cup angle (Degrees)	25	25
Length of the roller element (Inches)	0.6	1.2
Minimum diameter of the roller element (Inches)	0.6	0.4
Number of rollers	14	6

The results obtained for the objective functions are shown in Table 8-5.

Table 8-5: Objective functions' values for the new bearings

Objectives	Values	
	Back Bearing	Front Bearing
Lifetime (million revolutions)	35	3
Lifetime (hours for the bit's speed of 110 rpm)	2625	225
Factor of safety for static loading	2.8	1.2

Chapter 9
Bearing and Seal Integrated Design

9.1 Outline

In this chapter, a brief explanation of the features of the new design of tapered bearings is presented, providing some general information about the new elements and some instructions for assembling the elements.

9.2 The New Design of Tapered Bearings and Seal

Figure 9-1 shows the new design of the bearing and seal.

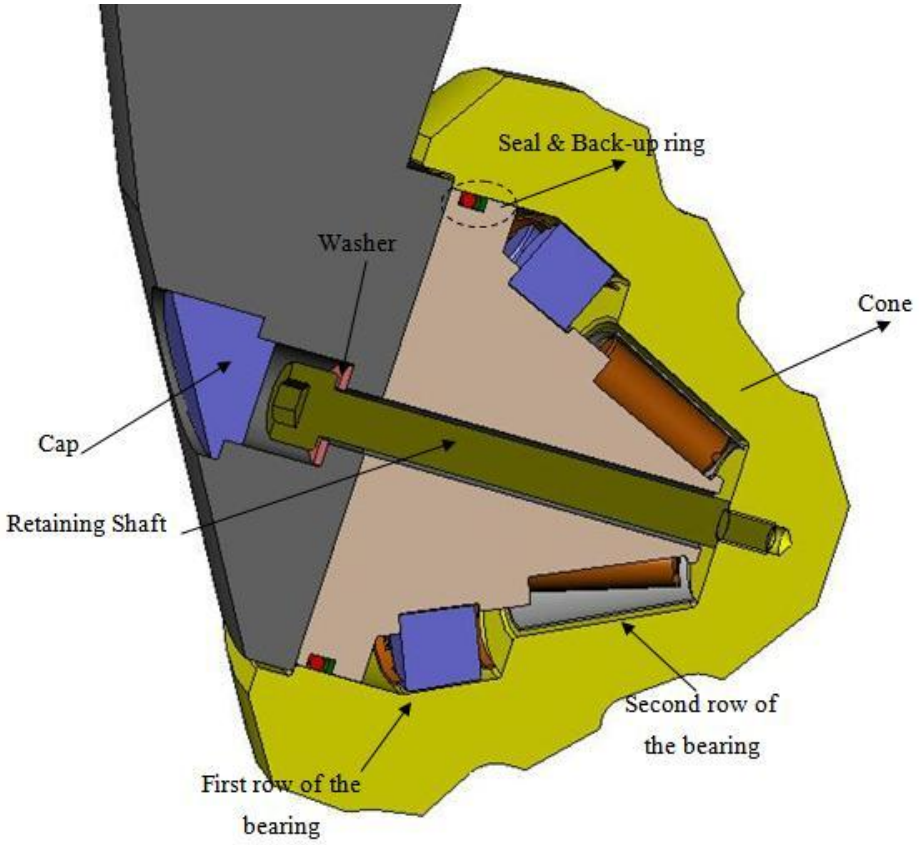

Figure 9-1: New design of the bearing and seal

9.3 New Cone

The inside profile of the cone has been changed according to the new bearing's design. In the new profile, there are some tapered surfaces, which are used as the outer race of the new tapered roller bearings. Tapered rollers, which form two different rows, are located between the arm's journal and these tapered surfaces. The new cone design is shown in Figure 9-2.

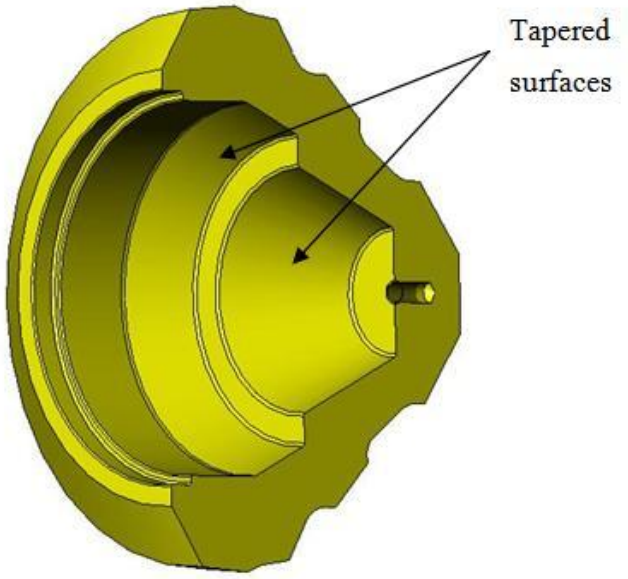

Figure 9-2: Cross section of new cone

9.4 New Arm's Journal

The arm's journal has also been adjusted to satisfy the new design. First, surfaces have been changed to a tapered shape to form the inner races of the new tapered bearing. There are two different rows for tapered rollers. For each row, the journal has two ribs: a higher rib in the back and a shorter one at the front. These two ribs prevent the rollers from moving axially. Another feature of the new arm's journal is a groove for the seal. Two different designs are provided with slightly different grooves. In the first design, an o-ring and a back-up ring are used, while in the second design the o-ring is replaced by a new S-profile seal, as addressed in 9.9. A diagram of the arm's journal is provided in Figure 9-3.

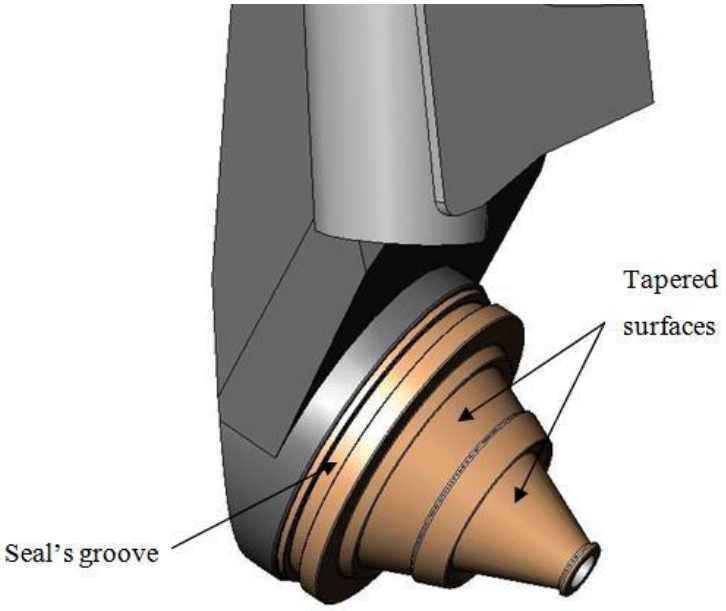

Figure 9-3: Arm's journal

9.5 Arm's Holes

A few changes should be made in the arm's design. In the new design there are no air holes, as the bearings are sealed; therefore, it is necessary to drill a new hole into the arm for the retaining shaft. Figure 9-4 shows the section view of this new hole.

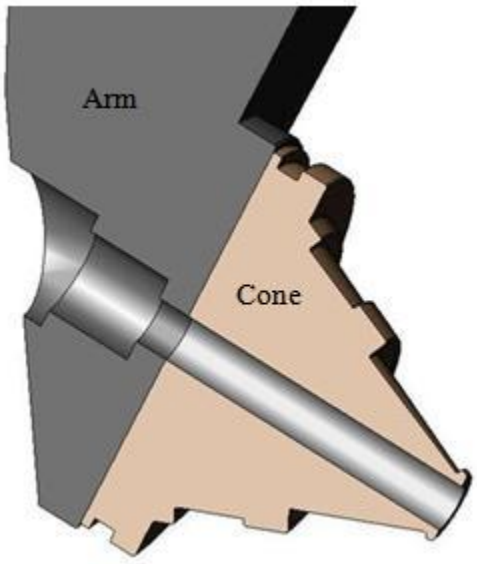

Figure 9-4: New arm's hole

9.6 Retaining Shaft

The retaining shaft is used to hold the cone in place while assembling the bit. In the previous method balls were used to retain the cone. A simpler method, which could reduce the cost of production by removing required balls, is used here. In this method, the shaft, which is threaded at the end, would be bolted to a tapped hole in the cone. The head of this shaft is seated on a rib in the arm, which prevents its axial motion. A thrust washer is placed between the rib and the head. The length of the shaft is such that it allows a very small axial motion for the cone and prevents the cone from being pushed against the arm's wall. A cap is used to cover the backend of the hole in the arm, while the downhole end is welded to ensure it is sealed. Figure 9-5 shows the proposed design of the retaining shaft.

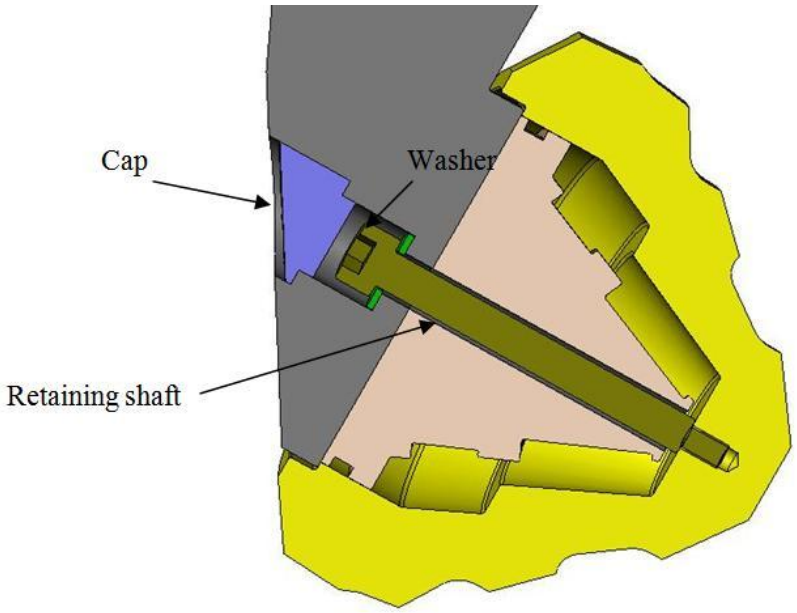

Figure 9-5: Retaining shaft, washer, and cap

The specifications of the washer outlined in Table 9-1.

Table 9-1: Flat washer's specifications

Specifications	Description
Type	Misumi Thrust Washer (LFZW)
Catalog no.	8
I.D.	10 mm
O.D.	18 mm
Thickness	1.5 mm

9.7 Tapered Rollers

In the new design, tapered rollers with two different specifications were used, as specified in Table 9-2. Figure 9-6 shows the new tapered rollers design. As with current design, the bearings' surfaces are greased during installation.

Table 9-2: Tapered rollers' specifications

Specifications	Roller 1	Roller 2
Maximum diameter (inch)	0.62	0.44
Length (inch)	0.60	1.2
Roller's angle (degree)	2	2
Crowning radius (inch)	0.02	0.02
Number of rollers per each arm	11	5
Material	AISI S-2	

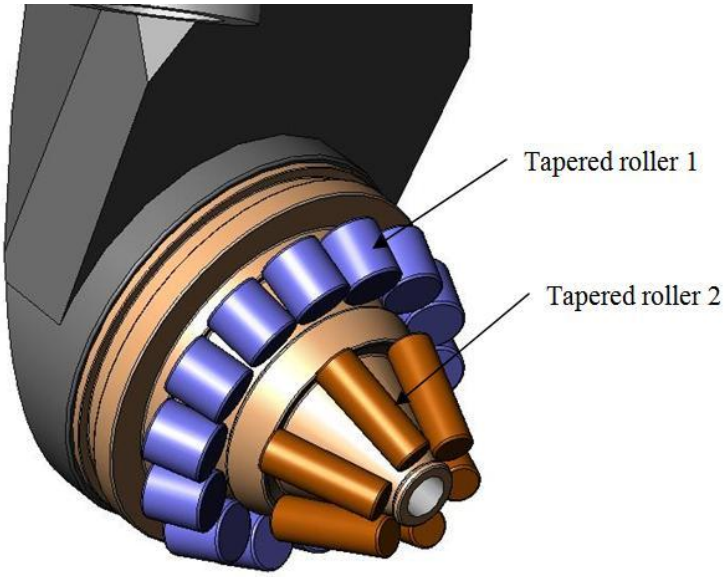

Figure 9-6: New tapered rollers

9.8 Cages

The cages are used to hold the rollers in place and prevent contact, which can reduce their life. Three different types of cages are used for tapered roller bearings, including stamped steel cages, machined cages, and pin type cages. Two methods are commonly used to install the cage and rollers over the inner race of tapered roller bearings. In the first method, the cage is slightly expanded by means of special tools and is then slid over the inner race. In the second method, the cage is positioned over the inner race and

the rollers are then snapped to the openings of the cage. For pin type cages, the pins can be easily inserted after installing all pieces. Figure 9-7 shows a tapered pressed steel cage.

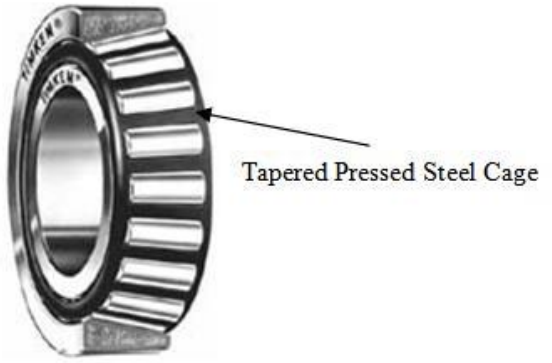

Figure 9-7: A Steel cage for tapered roller bearings

The new designed cages can be fabricated by two different methods, as shown in Table 9-3. When installing the new cages, they must be placed in appropriate rows; the rollers can then be inserted by snapping them into place. Figure 9-8 shows the new designed cages.

Table 9-3: Fabrication methods for the cages

Method	Material	Wall Thickness (inch)
Metal Stamping	Steel sheet	0.0209 inch (Gauge No.25)
Molding	Glass fiber	0.1

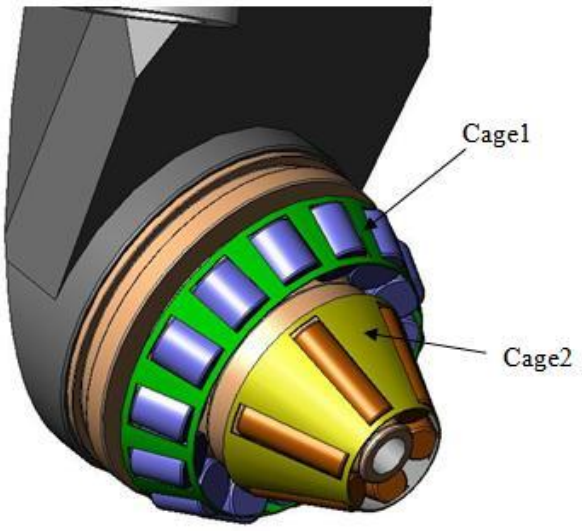

Figure 9-8: New designed cages

9.9 Seals

As mentioned before, elevated pressures while drilling result in premature damage to the seals. Using seals capable of withstanding higher pressures can address this problem. Such pressures vary from hundreds of psi for blasthole drilling to thousands of psi for oil drilling. The new design includes two different types of seal which can be employed upon the application.

Two seals proposed here can withstand different levels of pressure. The first type of seals uses simple o-ring, which can withstand pressures up to 5000 psi. The second seal is a new type of seal specifically designed for high pressure-high temperature environments, which can bear higher pressures of up to 20000 psi. The groove's dimensions for the two different types of seals are slightly different and both designs are provided here. For both methods, a back-up ring of the same material and size is used to prevent the seal's extrusion. The main seal is placed between pressure and the back-up ring. The selected materials for elastomers have been highlighted in Table 9-4 and Table 9-5.

For the s-profile seal, the material is a type of fluorocarbon elastomer seals and is able to withstand temperatures of up to 400 *F* and for the o-ring EPM, the material is a copolymer of ethylene and propylene which again bears temperatures up to 400*F*.

Table 9-4: O-ring's specifications (Parker)

Specifications	Description	
Application	Low Pressure Environments	
Model	*Size*	2-239
	I.D.	3.609 inch
	W	1/8 inch
Maximum pressure	5,000 psi	
HTHP Elastomers	*Type*	*Maximum Temperature (F)*
	EPM	**400**
	AEM	325
	ECO	275
	NBR	250
Back-up Rings	Parbak Elastomer	
	PTFE	
	Metal Non-Extrusion	

Table 9-5: S-Seal's specifications (Parker)

Specifications	Description	
Application	High Pressure/High Temperature (HTHP) Environments	
Model	*Size*	2-239
	I.D.	3.609 inch
	W	1/8 inch
Maximum pressure	20,000 psi	
HTHP Elastomers	*Type*	*Maximum Temperature (F)*
	V1238-95	**400**
	N4007-90	325
	N4027-90	275
Springs	Stainless Steel	
	Inconel (NACE spec MR-01-75)	

Figure 9-9 to Figure 9-11 show the new designs for sealing.

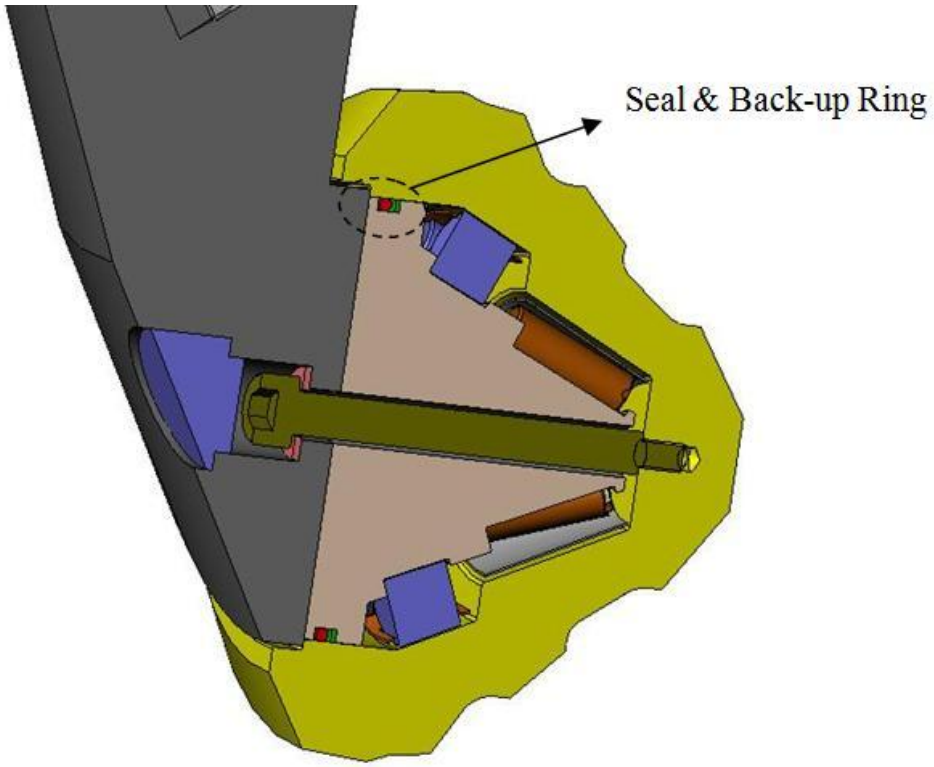

Figure 9-9: Seal and back-up ring's position

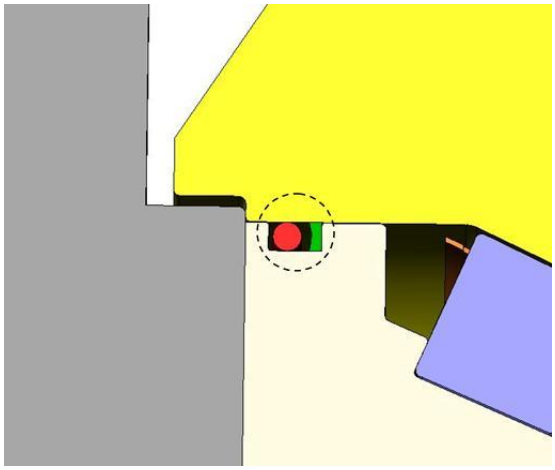

Figure 9-10: O-ring and back-up's cross section

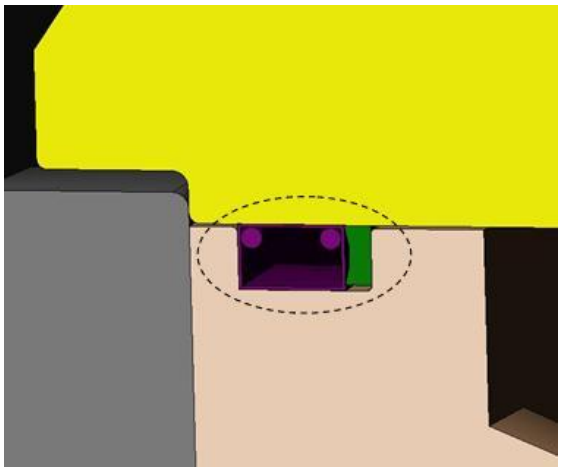

Figure 9-11: S-Seal and back-up's cross section

Chapter 10
Experimental Set-Up

10.1 Application

The purpose of the experimental set-up is to test the performance of the new sealed tapered bearings and the new insert pattern of the cones. These tests can be used to evaluate and improve the proposed designs. The experimental apparatus consists of a drum filled with water which is pressurized by air to test the durability of the bearings. The cone is rotated by a hydraulic motor located outside the drum and is pressed downward by a hydraulic cylinder. These conditions simulate the harsh environment in which the bits typically work. Moreover, while the bit rotates, the vibrations induced due to the contact between the inserts and the drum's base can imitate the vibrations generated by bit-rock interaction while drilling. Measurements can be made to determine if the new design is effective in reducing the vibrations.

10.2 Description

The set-up consists of five main subsystems: pressing unit, test unit, air pressurizing unit, power unit, and control unit. The test unit is installed on a hydraulic press and is connected to a hydraulic motor and air pressurizing unit, as shown in Figure 10-1. Therefore, the main part of the set-up includes the test unit and its components, while the other subsystems are standard parts and are not dealt with in this section.

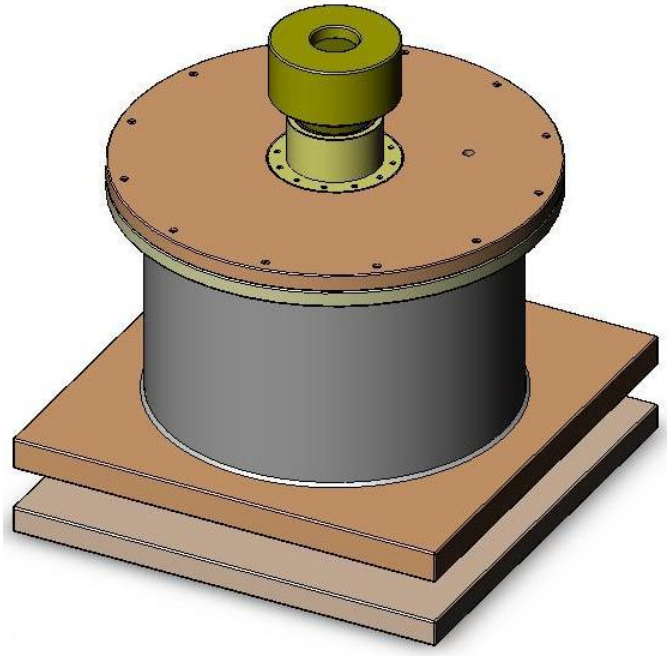

Figure 10-1: The experimental set-up

The test unit can also be divided into four subsystems: drum, pressing unit, power transmission unit, and hooking arm as shown in Figure 10-2 and Figure 10-3. In this section, each one of these subsystems and their applications are described.

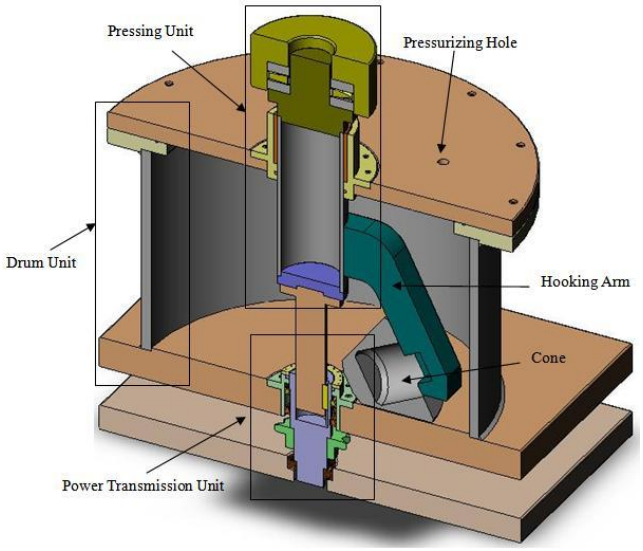

Figure 10-2: Test unit's subsystems

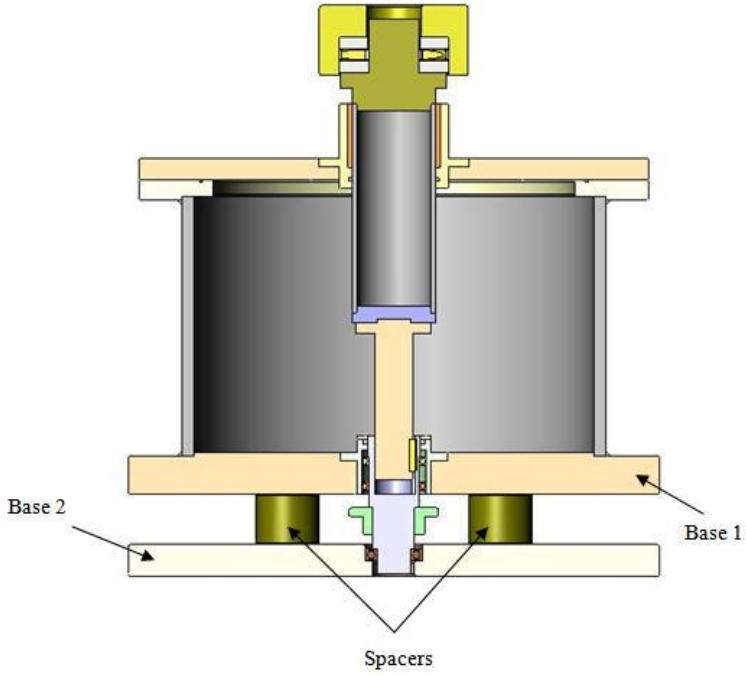

Figure 10-3: The base of the test unit and the spacers

10.3 Drum

The purpose of the drum is to provide a harsh environment for the tests, as shown in Figure 10-4. The drum consists of a pipe, which is welded at the bottom to the base. The base, which represents the bottom of the drum, is connected to a housing unit, which holds the power transmission unit's components. On top, a cap is placed on a flange that is welded to the pipe. This cap can easily be lifted by the upward motion of the hooking arm while changing the cone or filling the drum with water. The cap is connected to a housing unit in the center, which hosts the pressing unit's components, and is fastened to the flange by the bolts with an o-ring sealing the cavity between them.

The drum can be filled by water or special drilling liquid to test the sealing and bearing performance. A hole is drilled in the cap to provide the connection to the air pressurizing unit. When the drum is filled near to the top, the air pressurizing unit compresses the remaining air inside providing the desired pressure for tests.

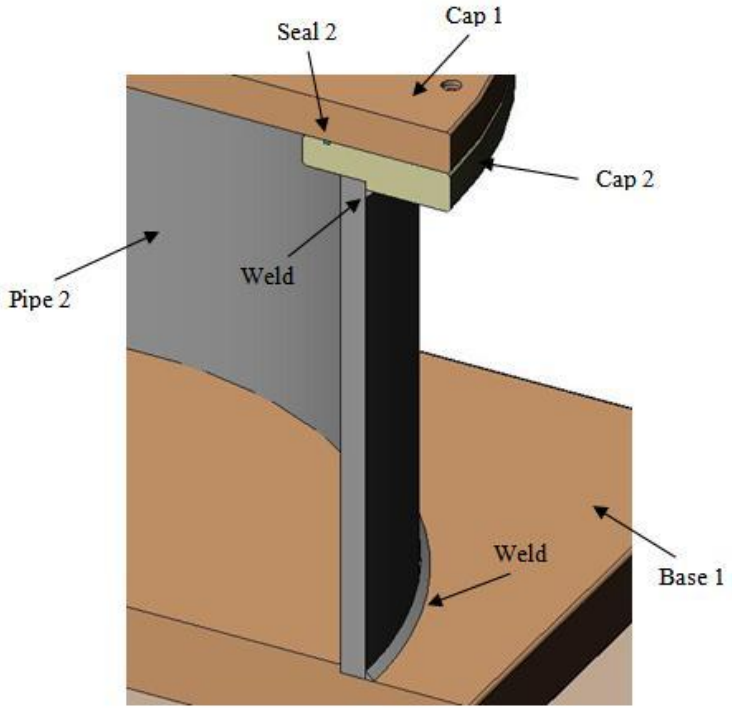

Figure 10-4: The drum of the test unit

10.4 Pressing Unit

The pressing unit provides a structure which permits downward force on the cone, while also allowing the cone to rotate, as shown in Figure 10-5. This specific structure resembles the real operating conditions of

rotary cone bits, which involve rotation while being pushed downward simultaneously. The components of the pressing units are: the head, thrust bearing, pipe and its components, housing unit, brass bushing, and seal.

The head is connected to the bottom of the hydraulic cylinder and is pressed against the thrust bearing. A pipe has been used to transmit pressing force downward. Using a pipe instead of a complete shaft can reduce the required amount of material. The top and the bottom of this pipe are welded to the cap and the base. The thrust bearing also lands on the pipe's cap. The pipe moves inside a brass bushing, which works as a radial bearing that allows directional motion of the pipe. The bushing is held inside a housing, which is connected to the cap of the drum by means of bolts. An o-ring located at the bottom of the housing unit seals the cavity between the drum and the pipe.

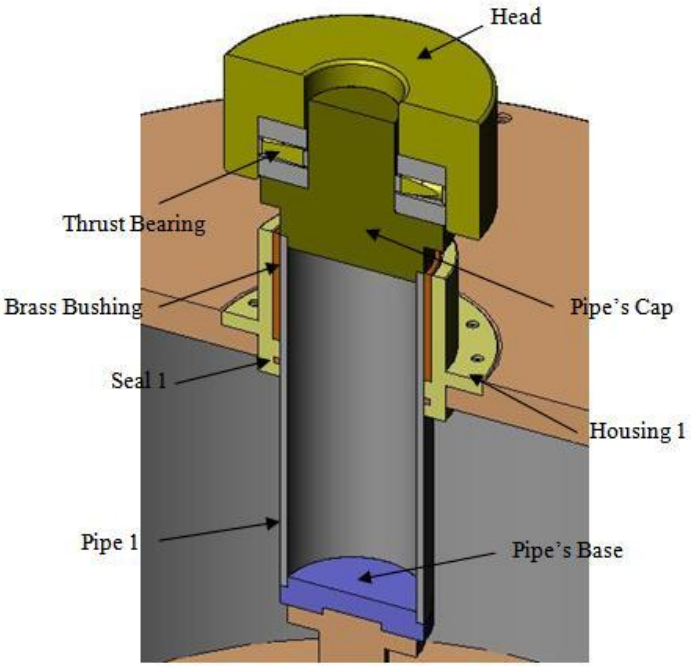

Figure 10-5: The pressing unit

10.5 Power Transmission Unit

The power transmission unit transfers the rotary motion from a hydraulic motor to the hooking arm, as shown in Figure 10-6. This unit consists of: the central shaft, power transmitting shaft, sprocket, housing unit, and wiper. The central shaft is connected to the pipe's base of the pressing unit by bolts and is connected to the power transmitting shaft by a key. The power transmitting shaft has a hollow portion at the end which includes a key housing. This configuration allows the central shaft to move up and down

with pressing the bottom of the drum. The power transmitting shaft is connected to a sprocket which can be connected to the hydraulic motor by a chain. The sprocket is positioned in the space provided between the two bases by means of spacers. A housing unit bolted to the upper base holds the whole unit. At the top, it has a wiper which can effectively seal the liquid inside and keep it from leaking. All bearings are press fitted into their housings.

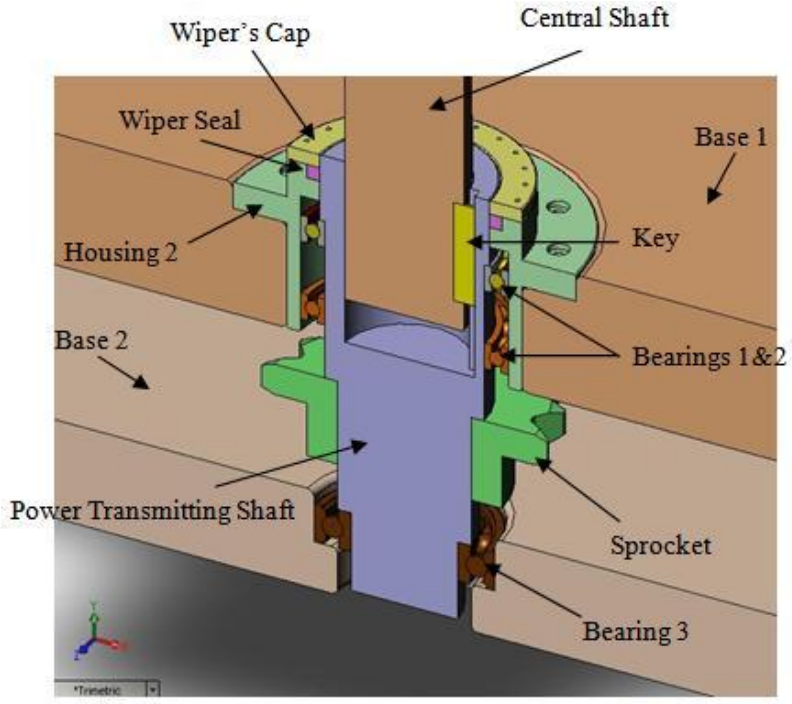

Figure 10-6: The power transmitting unit

10.6 Standard Parts

Table 10-1 shows the standard parts used in the experimental set-up.

Table 10-1: Standard parts of the experimental set-up

Part	Specifications
Wiper	Parker type H (8600) double lip wiper rings
Pipe	3 ½ inches steel pipe
Bearings 1&2	SKF 61812
Bearing on the base	SKF 6008
Thrust bearing	SKF 89412 TN
Sprocket	Misumi SP60B-16-50

10.7 Acknowledgment

I would like to thank Jason Sears, a student for the Conestoga College at Waterloo who co-operated with me on this part of the project. The designs of the hooking arm and the drum's pipe are adopted from his design, although some minor modifications have been made; although some minor refinements have been made.

Chapter 11
Conclusions and Future Work

11.1 Insert Pattern Optimization

11.1.1 Discussions

The results demonstrate that the irregular distribution of inserts on the cones can dramatically reduce the total vibratory energy induced by the bit-rock interactions. Such results were expected, as explained in Chapter 4, since tuning the timings between the repeated impulses results in damping out the amplitude of vibrations. As presented in the previous sections, the configurations are unique for each rotary speed. This can also be explained in terms of the characteristics of the "response" and the "timing between the impulses"; while the response remain identical for all rotary speeds and the timing changes due to the change in the rotary speed of the drillstring. The optimum configurations can be found to reduce the total vibratory energy across a range of operating speeds.

An even distribution of inserts generates an excitation pattern with a specific frequency. For various numbers of inserts and rotary speeds, such a frequency may be close to one of the natural frequencies of the system. In such cases, the effect of irregular configuration of inserts on the total vibratory energy of the system becomes even more obvious, as it eliminates the chance of resonance in the system. For example, considering a 20-insert row with 150 *rpm*, the frequency for the even distribution of inserts is equal to 100 *Hz*, which is almost identical to the second natural frequency of the system for axial vibrations. For this case, the irregular configuration dramatically reduces the total vibratory energy of the system by an amount of 84%.

11.1.2 Recommendations

Some refinements can be made in the different steps of this analysis to improve the results. The finite element model can be refined in different ways to generate more accurate results. for example, coupling between different modes can be considered in order to obtain a more comprehensive analysis for overall drillstring vibrations. Contact with the borehole wall also can be taken into account to add nonlinear features to more closely resemble the actual system behavior. The number of elements in the model can also be increased to refine the results.

A detailed study should be conducted to clarify the nature of insert-rock interactions. Finite element analyses can be very helpful to gain some insight into the structural behavior of these interactions.

Moreover, some investigations can be made based on those analyses to include the differences between excitation mechanisms for different modes of vibrations.

The optimization criteria can also be changed to improve upon the current results. New objective functions can be tried to address more features of drillstring vibrational behavior. The constraint can also be defined in such a way as to include other effects; for example, fracture mechanics criteria for crushing the rock. Other optimization methods can be compared to the genetic algorithm method to increase the optimization process' efficiency in terms of the processing time.

Finally, conducting appropriate experiments can be helpful to evaluate the simulation results. The experimental set-up designed for this project can be used to address these recommendations. It is also very helpful to use designed experiments for further investigations. This method helps to clarify the effects of different parameters on the system vibrations, especially for those aspects which cannot be easily simulated by means of mathematical models.

11.2 Bearing and Seal Design

11.2.1 Discussions

The new design for bearings and seals can address the problems that reduce bearings' lifetime and performance. Tapered roller bearings can withstand elevated forces for longer durations, while the new cages eliminate contact between rollers, resulting in better performance and longer life of the bearings. The new retaining method also reduces the number of elements used for rotary cone bits, while maintaining the required holding task. The seals can keep the debris from entering the bearing cavity and are able to operate in harsh environments.

11.2.2 Recommendations

Although the greasing proposed in the new design is capable of maintaining the lubricating function to an acceptable extent, it is recommended that an appropriate lubricating and cooling system be developed, which could extend the operational lifetime of the bearings. Such a lubrication system could use the rotary motion of the roller cones to circulate the lubricant inside the passages. It could also contain a multi-fin reservoir located in an appropriate place to be cooled by the flow of air or a drilling mud. The passageways could then be designed to deliver the lubricant to the required areas with a higher cooling performance.

Appendix

Appendix A

Derived formulas for bearing design

The formulas for the bearing design section were derived or rearranged as shown below:

Rearranged formulas for bearing design
$\tan\left(\frac{\alpha_o + \alpha_i}{2}\right) = \frac{0.5 d_m}{w_1}$
$\alpha_R = \alpha_o - \alpha_i$
$D_{max} = 2 l_t \tan\left(\frac{\alpha_o - \alpha_i}{2}\right) + D_{min}$
$R_{max} = (0.5 d_m + l_t \sin(\alpha_R/2))/\cos\left(\frac{\alpha_o + \alpha_i}{2}\right)$
$Z = \frac{2\pi R_{max}}{D_{max}}$
$R'_{max} = R_{max} + \frac{D_{max}}{2}$
$d'_{max} = R'_{max} \cos\left(\frac{\alpha_o + \alpha_i}{2}\right)$
$R_{min} = (0.5 d_m - l_t \sin(\alpha_R/2))/\cos\left(\frac{\alpha_o + \alpha_i}{2}\right)$
$R'_{min} = R_{min} + \frac{D_{min}}{2}$
$d'_{min} = R'_{min} \cos\left(\frac{\alpha_o + \alpha_i}{2}\right)$

Bibliography

Timken. http://www.timken.com/en-us/Pages/home.aspx (accessed July 15, 2008).

Parker. http://www.parker.com/portal/site/PARKER/ (accessed July 15, 2008).

Sandvik. http://www.sandvik.com/ (accessed July 15, 2008).

Production Enhancment Systems. http://www.sappsticks.com/ez-string.shtml (accessed July 15, 2008).

California Department of Conservation. http://www.conservation.ca.gov/ (accessed July 15, 2008).

Baker Hughes. http://www.bakerhughes.com/ (accessed July 15, 2008).

Abbassian, F., and V.A. Dunayevsky. "Application of Stability Approach to Torsional and Lateral Bit Dynamics." *SPE Drilling & Complettion*, June 1998: 99-107.

Altintas, Y., S. Engin, and E. Budak. "Analytical Stability Prediction and Design of Variable Pitch Cutters." *Journal of Manufacturing Science and Technology, Transactions of the ASME* 121 (May 1999): 173-178.

"American National Standard Institute, American National Standard (ANSI/AFBMA), Standard 11-1990: "Load Ratings and Fatigue Life for Roller Bearings"."

Ashley, D.K., X.M. McNary, and J.C. Tomlinson. "Extending BHA Life with Multi-Axis Vibration Measurments." *SPE/IADC Drilling Conference.* Amsterdam, 2001.

Bailey, J., and I. Finnie. "An Amalytical Study of Drillstring Vibration." *Journal of Engineering for Industry, Transaction of the ASME* 82 No.2 (1960): 122-128.

Besaisow, A., and M. Payne. "A Study of Excittaion Mechanisms and Resonances Including Bottomhole-Assembly Vibrations." *SPE Drilling Engineering* 3 No.1 (1988): 93-101.

Brakel, J.D. *Prediction of Wellbore Trajectory Bottom Hole Assembly and Drilling Dynamics.* Tulsa: University of Tulsa,The Graduate School, PhD Thesis, 1986.

Brett, J.F. "The genesis of Torsional Drillstring Vibrations." *SPE Drilling Engineering*, September 1992: 168-174.

Carre, L., et al. "Application of New Generation large Roller-Cone Bits Reduces Drilling Costs in eastern Venezuela." *SPE Latin American and caribbean petrolum Engineering Conference.* Buenos Aires, 2001. SPE 69617.

Chen, S., and M. Geradin. "An Improved Transfer Matrix Technique as Applied to BHA LAteral Vibration Analysis." *Journal of Sound and Vibration* 185 No.1 (1995): 93-106.

Chen, S.S., M.W. Wambsganss, and J.A. Jendrzejzyk. "Added Mass and Damping of a Vibrating Rod in Confined Viscous Fluids." *Journal of Applied Mechanics, Transactions of the ASME* 43 No.2 (1976 Series E): 325-329.

Chevallier, A. *Nonlinear Stochastic Drilling Vibrations.* Houston: Rice University, Department of Mechanical Engineering and Material Science, PhD Thesis, 2000.

Christofforou, A., and A. Yigit. "Dynamic Modeling of Rotating Drillstrings With Borehole Interactions." *Journal of Sound and Vibration* 206 No.2 (1997): 243-260.

Daly, J.E. Valve assembly for drill bit lubrication system. Patent US 4452323. June 5, 1984.

Dareing, D. "Drill Collar Length is a Major Factor in Vibration Control." *Journal of Petroleum Technology* 36 No.4 (1984): 637-644.

Dareing, D., Livesay, B. "Longitudinal and Angular Drill-String Vibrations with Damping." *Journal of Engineering for Industry, Transaction of the ASME* 90 No.1 (1968): 54-61.

Dawson, R., Y.Q. Lin, and P.D. Spanos. "Drill String Stick-Slip Oscillations." *Proceedings of the 1987 SEM Spring Conference on experimental Mechanics.* Houston, 1987. 590-595.

Delgado, S.R., R.J. kotch, and F. Hall. Pressure compensator for drill bit lubrication system. Patent US 5072795. December 17, 1991.

Dick, A.J., and C.C. Lin. Hydrodynamic pump passages for rolling cone drill bit. Patent US 7128171 B2. October 31, 2006.

Dykstra, M.L. *Nonlinear Drill String Dynamics.* Tulsa: University of Tulsa, The Graduate School, PhD Thesis, 1996.

Elsayed, M.A., D.W. Dareing, and C.A. Dupuy. "Effect of Downhole Assmebly and Polycrystalline Diamond Compact (PDC) Bit Geometry on Stability of Drillstrings." *Journal of Energy Resources Technology* 119 (1997): 159-163.

Frohrib, D., and R. Plunkett. "The Free Vibrations of Stiffened Drill Strings with Static Curvature." *ASME Journal of Engineering for Industry* 89 No.1 (1967): 23-30.

Grimes, B., and B. Kirkpatrick. "Step Change in Performance: Upgraded Bit Technology Significantly." *The 2006 SPE Annual Technical Conference and Exhibition.* San Antonio, 2006.

Halsey, G.W., A. Kyllingstad, T.V. Aarrestad, and D. Lysne. "Drillstring Torsional Vibrations: Comparison Between Theory and Experiment on a Full-Scale Research Drilling Rig." *SPE paper 15564 presented at the 1986 SPE Annual Technical Conference and exhibition.* New Orleans, 1986.

Harris, T.A. *Rolling Bearing Analysis.* 4th. NewYork: Jon Wiley $ Sons, 2001.

Hixon, C.E. Rock drill bit lubricant circulating system. Patent US 5099932. March 31, 1992.

Hooper, M.E. Lubricant system for a rotary cone rock bit. Patent US 5265964. November 30, 1993.

"Inernational Standard ISO 76, "Rolling Bearings-Static Load Ratings"." 1989.

Jansen, J.D., and L. Van den Steen. "Active Damping of Self-Excited Torsional Vibrations in Oil Well Drillstrings." *Journal of Sound and Vibration* 179, no. 4 (1995): 647-668.

Karlsson, L. Rotary drill bit having filling openning for the installation of cylinderical bearings. Patent US 6250407 B1. June 26, 2001.

Keller, W.S., and W.D. Vanderford. Thrust flange actuated rock bit lubrication system. Patent US 4181185. January 1, 1980.

Kreisle, L., and L. Vance. "Mathematical Analysis of the Effect of a Shock Sub on the Longitudinal Vibrations of an Oilwell Drill String." *Society of Petroleum Engineers Journal* 10 No.4 (1970): 349-356.

Leine, R.I., D.H. Van Campen, and W.J.G Keultjes. "Stick-slip Whirl Interaction in Drillstring Dynamics." *Journal of Vibration and Acoustics* 124 (2002): 209-220.

Levefelt, B.G. Roller bit seal excluded from cuttings by air discharge. Patent US 4183417. January 15, 1980.

Lin, C.C. Mud debris diverter for earth-boring bit. Patent US 7066287 B2. June 27, 2006.

Lin, C.C. PDC face seal for earth-boring bit. Patent US 7128173 B2. October 31, 2006.

Lin, Y.Q., and Y.H wang. "Stick-Slip Vibration of Drill Strings." *Journal of Engineering for Industry, Transaction of the ASME* 113 (February 1991): 38-43.

Mcleod, S.A., T.T. O'Grady, E.C. Sullivan, J.S. Mason, and C. Lin. "Application of Metal-Bearing Seal roller-Cone Bit Reduce Rig Time/drilling Costs in Green Canyon, Depp Water Golf of Mexico." *The 2000 IADC/SPE Drilling Conference*. New Orleans, 2000.

McQueen, R.W. Viscous pump rock bit lubrication system. Patent US 4167219. September 11, 1979.

Morris, W.A. Rotary earth boring drill and method of assembly thereof. Patent US 4157122. June 5, 1979.

Mourik, N., and C. Cawthorne. Rock bit seal with extrusion prevention member. Patent US 6820704 B2. November 23, 2004.

Nguyen, D.Q. Anti-mud packing seal gland. Patent US 7086487 B2. August 8, 2006.

Nguyen, D.Q., T.J. Koltermann, G.L. Ricks, M.E. Morris, C.M. McCarty, and C.C. Lin. Gage surface scraper. Patent US 7066286 B2. June 27, 2006.

Olschewski, A., M Brandenstein, and L. Walter. Rotary drill bit with conical rotary cutters. Patent US 4367904. January 11, 1983.

Pao, L. "Multi-input Shaping Design for Vibration Reduction." *Automatica* 35 (1999): 81-89.

Pao, L., and W. Singhose. "A Comparison of Constant and Variable Amplitude Command Shaping Techniques for Vibration Reduction." *Proceedings of the 4th IEEE Interntional Conference on Control Applications.* Albany, NY, USA, 1995. 875-881.

Paslay, P., and D. Bogy. "Drill String Vibrations Due to Intermittent Contact of Bit Teeth." *Journal of Engineering for Industry, Transactions of the ASME* 85 No.2 (1963).

Paslay, P., Y. Jan, J. Kingman, and J. Macpherson. "Detection of BHA lateral Resonances While Drilling With Surface Longitudinal and Torsional Sensors." *SPE 67th Annual Conference and Exhibition.* Washington, 1992. SPE 24583.

Payne, M.L. *Drilling Bottom-Hole Assmebly Dynamics.* Houston: Rice University, Department of Mechanical Engineering, PhD Thesis, 1992.

Persson, E.A. Bearing means in rotary drill bits. Patent US 4304444. December 8, 1981.

Phelan, C.M. Drill bit lubricant circulation system. Patent US 4390072. June 28, 1983.

Portwood, G.R., C.E. Cawthorne, R.H. Slaughter, R. Didericksen, P. Cariveau, and R. Denton. Dual-seal pressure communication system. Patent US 6679342 B2. January 20, 2004.

Przemieinecki, J.S. *Theory of Matrix Structural Analysis.* NewYork: mcGraw-Hill Book Company, 1968.

Rao, S. *Mechanical Vibrations.* 4th. New Jersey: Pearson education, 2004.

Richard, Thomas, Christophe Germay, and Emmanuel Detournay. "A simplified model to explore the root cause of stick-slip vibrations in drilling systems with drag bits." *Journal of Sound and Vibration* 305 (2007): 432-456.

Rives, A.K. Drill bit lubricant apparatus and method. Patent US 7240745 B1. July 1, 2007.

Serrarens, A.F.A., M.J.G Van de Molengraft, J.J. Kok, and L. Van den Steen. "H-infinity Control for Suppressing Stick-Slip in Oil Well Drillstrings." *IEEE Control Systems*, Aprill 1998: 19-30.

Shirase, K., and Y. Altintas. "Cutting Force and Dimensional Surface Error Generation in Peripheral Milling with Variable Pitch Helical End Mills." *International Journal of Machine Tools and Manufacturing* 36 No.5 (May 1996): 567-584.

Singer, N., and W. Seering. "Design and Comparison of Command Shaping Methods for Controlling Residual Vibration." *IEEE International Conference on Robotics and Automation.* Scottsdale, 1989. 888-893.

Singer, N., and W. Seering. "Preshaping Command Inputs to Reduce System Vibration." *Journal of Dynamic Systems, Transactions of the ASME* 112 No.1 (1990): 76-82.

Singer, N., W Singhose, and E. Kriikku. "An Input Shaping Controller Enabling Cranes to Move Without Sway." *Proceeding of ANS Seventh Topical Meeting on Robotics and Remote Systems.* Augusta, 1997. 225-231.

Singhose, W., W. Seering, and N. Singer. "Shaping Inputs to Reduce Vibration: A Vector Diagram Approach." *Proceedings of the IEEE International Conference on Robotcs and Automation.* Cincinnati, 1990. 922-927.

Slaughter, R.H., P.T. Cariveau, R. Didericksen, and W.M. Conn. Protected lubricant reservoir with pressure control for sealed bearing earth boring drill bit. Patent US 6206110 B1. March 27, 2001.

Slavicek, J. "The Effect of Irregular Tooth Pitch on Stability of Milling." *Proceeding of the 6th MTDR Conference.* London: Pergamon Prees, 1965. 15-22.

Spanos, P., A. Chevallier, and N. Politis. "Nonlinear Stochastic Drill-String Vibrations." *Journal of Vibration and Acoustic, Transaction of the ASME* 124 (October 2002): 512-518.

Spanos, P., A. Sengupta, R. Cunningham, and P. Palsay. "Modeling of Roller Cone Bit Lift-Off Dynamics in Rotary Drilling." *Journal of Energy Resources Technology* 117, no. 2 (1995): 115-124.

Spanos, P., M. Payne, and C. Secora. "Bottom-Hole Assembly Modeling and Dynamic Response Determination." *Journal of Energy Resources Technology* 119, no. 3 (1997): 153-158.

Tzes, A., and S. Yurkovich. "An Adaptive Input Shaping Control Scheme for Vibration Suppression in Slewing Flexible Structures." *IEEE Transactions on Control Systems Technology* 1 No.2 (1993): 114-121.

Urbieta, A., et al. "Advanced Technology Improves Drilling Economics/Sets New Benchmark, Southeast Mexico." *The First international oil Conference and Mxhibition in Mexico.* Cancun, 2006. SPE 103921.

Villaloboz, A.A. Rock bit bearing structure. Patent US 4061376. December 6, 1977.

Walters, D.F. Cutter actuated rock bit lubrication system. Patent US 4183416. January 15, 1980.

Warren, T.M. "Factors Affecting Torque for a Roller Cone Bit." *Journal of Petrolum Technology,* September 1984: 1500-1508.

Yong, Z, and D.P. deRimanoczy. Dynamic seal with soft interface. Patent US 7117961 B2. October 10, 2006.

Zahradnik, A.F., E.C. Sullivan, C. Lin, T.J. Koltermann, and S.R. Schmidt. Earth-boring bit with improved bearing seal. Patent US 6142249. November 7, 2000.

Zamanian, M., S.E. Khadem, and M.R. Ghazavi. "Stick-slip oscillations of drag bits by considering damping of drilling mud and active damping system." *Journal of Petroleum Science & Engineering* 59 (2007): 289-299.